

DESIGN AND DEVELOPMENT OF A METAL ADDITIVE MANUFACTURING SYSTEM TO FABRICATE COMPONENTS

200159X S.C.P. Ephraims

200024F K.S. Amarasekara

200055B A.G.C.O. Atadaswala

Advised by

Prof. N.D. Jayaweera

Department of Mechanical Engineering

University of Moratuwa

Dr. A.T.H.E. De Silva

Department of Mechanical Engineering

University of Moratuwa

Dr. Tamasha Samarasinghe

Department of Mechanical Engineering

University of Moratuwa

Report submitted in partial fulfilment of the requirements for the degree of Bachelor of
Science in Engineering

Department of Mechanical Engineering

University of Moratuwa

Sri Lanka

July 2025

DECLARATION

We declare that this is our own work, and this report does not incorporate without acknowledgement any material previously submitted for a Degree or Diploma in any other University or institute of higher learning and to the best of my knowledge and belief it does not contain any material previously published or written by another person except where the acknowledgement is made in the text.

Also, we hereby grant to University of Moratuwa the non-exclusive right to reproduce and distribute our report, in whole or in part in print, electronic or other medium.

Signature:  Date: 06/07/2025

Signature:  Date: 06/07/2025

Signature: *Chalangana* Date: 06/07/2025

The above candidates have carried out the research included in this research under my supervision.

Signature of the supervisor: Date: 06/07/2025

Signature of the supervisor:  Date: 06/07/2025

Signature of the supervisor:  Date: 06/07/2025

ABSTRACT

The increasing demand for rapid, cost-effective, and customizable manufacturing has accelerated the development of metal additive manufacturing technologies. This project focuses on the design and development of a metal additive manufacturing system based on Wire Arc Additive Manufacturing (WAAM) using Metal Inert Gas (MIG) welding integrated with a gantry-based robotic motion platform. The aim is to fabricate metal components layer by layer with improved precision and mechanical reliability, while maintaining affordability for small and medium-scale industrial applications.

The system architecture includes a three-axis gantry mechanism driven by stepper motors, controlled through an open-source firmware (Marlin) and coordinated via G-code generated from 3D models using slicing software. MIG welding is selected due to its high deposition rate, wide material compatibility, and economic viability. To ensure optimal performance, a comprehensive analysis of welding parameters such as current, voltage, wire feed rate, and travel speed was conducted. Additionally, simulations were performed using ANSYS DED to evaluate thermal behaviour, residual stress formation, and layer deformation during the metal deposition process. The insights gained from these simulations guided the selection of process parameters to improve build quality and dimensional accuracy. This system contributes to the ongoing development of low-cost, open-source metal 3D printing solutions, with potential applications in prototyping, repair, and small-scale production.

Key words: MIG Welding, WAAM, RAMPS

DEDICATION

This report is dedicated to the design and development of a low-cost metal additive manufacturing system utilizing MIG welding and a gantry robotic platform, with the aim of advancing accessible and practical solutions in the field of metal 3D printing and laying the groundwork for industrial innovation in Sri Lanka. We envision this work as a stepping stone for future generations of Sri Lankan engineers, encouraging them to explore the transformative potential of additive manufacturing technologies in reshaping traditional fabrication methods.

The successful integration of automated welding with motion control and simulation-based optimization marks a significant stride towards democratizing advanced manufacturing. It is our hope that this project sparks curiosity, nurtures innovation, and inspires continued research and development in the local manufacturing sector, ultimately contributing to Sri Lanka's journey toward self-reliance in industrial technologies and smart fabrication systems.

ACKNOWLEDGEMENTS

We would like to express our sincere gratitude to all those who contributed to the successful completion of this project.

This project was continuously enriched through the invaluable guidance and supervision of our project supervisors: Prof. N.D. Jayaweera, Dr. A.T.H.E. De Silva, and Dr. Tamasha Samarasinghe. Prof. N.D. Jayaweera provided us with continuous motivation, insightful advice, and unwavering support, inspiring us to seek innovative solutions throughout our research. Dr. A.T.H.E. De Silva offered vital direction in practical aspects of design, automation, and fabrication, significantly shaping the project's engineering foundation. Dr. Tamasha Samarasinghe played a key role in guiding us through the thermal and structural simulation aspects of the project, providing valuable feedback and motivation.

We also extend our gratitude to Dr. W.A.D.M. Jayathilaka, our final year project coordinator, for his support in managing the module workflow and for providing timely advice and assistance throughout the academic year.

A special thank you goes to Mr. Kevin for generously donating a brand-new RETOP MIG-275 welding machine, which was instrumental in the development and execution of this project.

We are also grateful to the non-academic staff of the Department of Mechanical Engineering for their assistance during the design, simulation, and manufacturing stages of the project.

Our heartfelt appreciation goes to our parents and families for their unwavering support, encouragement, and financial assistance, without which this journey would not have been possible.

Finally, we extend our deepest thanks to all individuals both directly and indirectly involved in this project over the past two semesters. Your contributions have been invaluable in making this endeavour a success.

TABLE OF CONTENTS

Declaration page of the candidate and supervisor	i
Abstract	ii
Dedication	iii
Acknowledgements	iv
Table of contents	v
List of Figures	ix
List of Tables	xi
List of abbreviations	xii
1 Introduction	13
1.1 Background	13
1.2 Motivation	13
1.3 Scope of the Project	14
1.4 Aim and Objectives	15
1.4.1 Aim	15
1.4.2 Objectives	15
1.5 Structure of the Report	16
2 Methodology	17
3 Literature Review	18
3.1 Additive Manufacturing Systems	18
3.1.1 Metal Additive Manufacturing	18
3.1.2 Powder Bed Fusion (PBF)	19
3.1.3 Material Jetting (MJ)	19
3.1.4 Binder Jetting (BJ)	19
3.2 Direct Energy Deposition Methods (DED)	20
3.2.1 Advantages of Direct Energy Deposition	21
3.2.2 Laser Metal Deposition (LMD)	22
3.2.3 Wire Arc Additive Manufacturing (WAAM)	22

3.3	Welding in WAAM Systems.....	24
3.3.1	Wire Arc Additive Manufacturing (WAAM)	24
3.3.2	Welding Parameters in WAAM.....	26
3.3.3	Welding Defects in WAAM	30
3.3.4	Welding Simulations in WAAM	34
3.3.5	Welding Testing Methods in WAAM.....	35
3.3.6	Tensile Testing.....	36
3.3.7	Non-Destructive Testing (NDT)	37
3.4	Comparison Between Welding Methods.....	38
3.5	Automating the System with Robot Systems.....	39
3.1	Overview of Robotic Systems in Additive Manufacturing (AM).....	39
3.2	Automation of the Welding Plant	42
3.2.1	Current and Voltage Control:.....	42
3.2.2	Wire Feed Rate:	42
3.2.3	Arc Length Control in the Welding Machine	42
3.3	Control Systems, Firmware, and Actuators	45
3.4	Research gap	47
4	Project Workflow.....	49
4.1.1	System Design and Development	49
4.1.2	Conceptual Design of the Printing System	49
4.1.3	Gantry System Architecture.....	51
4.1.4	Electrical and Firmware Setup.....	52
4.1.5	Welding Unit Integration	53
4.1.6	Slicing and G-code Generation.....	54
4.1.7	Workflow Automation and Control Flow.....	54
4.2	Manufacturing of the Setup.....	55

4.2.1	Fabrication of Structural Components	55
4.2.2	Installation of Motors, Rails, and Lead Screws	55
4.2.3	Torch Holder and Z-Axis Assembly	56
4.2.4	Cable Management and Safety Features	57
4.2.5	Integration and Full System Assembly	57
4.3	Process Parameters	58
4.3.1	Key Parameters: Voltage, Current, WFR, Travel Speed	58
4.3.2	Preliminary Manual Testing Results.....	58
4.3.3	Effects of Parameters on Bead Geometry	59
4.3.4	Empirical Calibration and Iterative Testing.....	59
4.3.5	Operating Envelope Identification	60
4.4	Simulation and Analysis.....	60
4.4.1	Simulation Objectives and Strategy	60
4.4.2	Geometry and Model Preparation	61
4.4.3	G-code Integration and Toolpath Definition.....	62
4.4.4	Thermal Analysis using ANSYS DED	62
4.4.5	Residual Stress and Deformation Prediction	63
4.4.6	Result Interpretation and Process Refinement	64
4.5	Control System Design.....	64
4.5.1	Gantry Motion Control	65
4.5.2	Starting Point Detection with Load Cell	65
4.5.3	Welding Torch Activation Using Extruder Signal.....	66
4.5.4	Real-Time Welding Current Measurement.....	67
4.5.5	Constant Arc Length Control.....	67
4.5.6	Control system Block Diagram for the Arc length correction system.....	69

4.5.7	Estimate a Linear Model for the Arc length correction system Using System Identification App	70
5	Experimental Test Results and Discussion	71
5.1	Experimental Fabrication and Validation	71
5.1.1	Material Selection and Test Samples	71
5.1.2	Printing Trials and Bead Formation	71
5.1.3	Visual and Dimensional Inspection	72
5.1.4	Cross-Sectional Analysis	73
5.1.5	Comparison with Simulated Results	74
5.1.6	Lessons Learned and Process Tuning	74
5.2	Discussion	74
5.2.1	Evaluation of System Performance	74
5.2.2	Parameter Influence and Process Stability	75
5.2.3	Comparison of Experimental vs Simulated Data	75
5.2.4	Practical Challenges and Solutions	75
5.2.5	Contributions and Implications for WAAM Development	76
5.2.6	Future work	76
6	Conclusions	76
	Reference	77
	Appendix	83

LIST OF FIGURES

Figure 3.1: Additive Manufacturing Processes [6]	18
Figure 3.2: Powder Bed Fusion	19
Figure 3.3: Binder Jetting	20
Figure 3.4: a) Wire Laser Additive Manufacturing (WLAM) b) Electron Beam Additive Manufacturing (EBAM) c), d) Wire Arc Additive Manufacturing (WAAM) [7]	23
Figure 3.5: WAAM system design concepts, University of Wollongong.[3]	26
Figure 3.6: a) Contour plot of cooling time $\Delta t_{8/5}$ as a function of heat input E and interlayer temperature T_i (quadratic regression model, model quality $R^2 = 98.6\%$); b) SEM images of the microstructures for two regions of the wall cross section of WAAM specimen V5 [25]..	28
Figure 3.7: Part of the actual weld bead in the experiment.[26]	30
Figure 3.8: The correlation between materials and defects in WAAM processes. [28]	33
Figure 3.9: 8 Axis articulated robot [35]	39
Figure 3.10 :5 DOF gantry robot system [3]	40
Figure 3.11: low-cost metal 3D printer [45]	41
Figure 3.12: Wire feed unit main circuit schematic [46].	42
Figure 3.13: Current and voltage sensing circuitry [48].	44
Figure 3.14 Experimental setup with a close-up image of the torch configuration consisting of thermal sensor, welding torch and laser triangulation [48].	44
Figure 3.15 The mounted circuit to the welding machine [48].	45
Figure 3.16 Components of the robot system [36]	45
Figure 3.17 Connections of Arduino 2560 [36].	45
Figure 3.18: Acceleration, velocity, and position as a function of time using a piecewise-constant jerk profile, which linearly increases the system's acceleration to a maximum value then decreases it again [36].	46
Figure 3.19: A comparison between the velocity of the X-axis without the ramping and with ramping [36].	47
Figure 4.1: Project Workflow	49
Figure 4.2: Steel Structure	51
Figure 4.3: Gantry System	51
Figure 4.4: RAMPS 1.4	52
Figure 4.5: Arduino MEGA	52
Figure 4.6: Retop MIG 275	53
Figure 4.7: Torch Mount	53
Figure 4.8: Pulley tensioning unit	56
Figure 4.9: Manufactured brackets	56

Figure 4.10: Z-Axis Assembly.....	56
Figure 4.11: Prototype	57
Figure 4.12: Geometry Models	61
Figure 4.13: Cartesian mesh	61
Figure 4.14: Thermal Simulation result After 300s Cool down for rectangular weld Bead....	62
Figure 4.15: Thermal Simulation Results After 4000s Cooldown for Circular Weld Bead....	63
Figure 4.16: Thermal Simulation Graph during Layer-by-layer metal deposition.....	63
Figure 4.17: Deformation Results for rectangular weld Bead	64
Figure 4.18: TMC 2209	65
Figure 4.19: Pronterface user Interface.....	65
Figure 4.20: Calibration Setup.....	66
Figure 4.21: Load Cell Mounting	66
Figure 4.22: Circuit diagram of the on-time increasing method.....	66
Figure 4.23: Load Cell Mounting	66
Figure 4.24: Setup to Read the extruder signal.....	66
Figure 4.25: Calibrated Values	67
Figure 4.26: The current display unit.....	67
Figure 4.27: Arc Length vs Welding Current	69
Figure 4.28: Control system block diagram in SIMULINK.....	69
Figure 4.29: Identification cycle	70
Figure 5.1: Circular Weld Bead	72
Figure 5.2: Prototype during the Welding	72
Figure 5.3: Wire Bead Thicknesses	72
Figure 5.4: High Travel Speed Weld Run	73
Figure 8.1: MATLAB code.....	84
Figure 8.2: MATLAB code to find the suitable arc lengths in different arc currents.....	84
Figure 8.3: Thermal Simulation.....	85
Figure 8.4: CAD Model	86
Figure 8.5: Gantry Control System.....	86
Figure 8.6: Fully Assembled Prototype	87
Figure 8.7: Steel Box Bar Structure	87
Figure 8.8: Front View of Assembly	87
Figure 8.9 : T002 Welding position 90-degree angle	88
Figure 8.10 : T001 Welding position 30-degree angle	88
Figure 8.11 : T002 Rectangular box in torch 90-degree perpendicular	89

Figure 8.12: T008, T009 and T0019 Welding beads	89
Figure 8.13: T005, T006 and T007 Welding bead.....	89
Figure 8.14: T001 Rectangular box in torch 30-degree angled.....	89
Figure 8.15: T005, T006 and T007 Welding bead.....	89
Figure 8.16: T001 Rectangular box in torch 30-degree angled	89
Figure 8.17: T011, T012, T013, T014 Welding Beads.....	89
Figure 8.18: T001 Rectangular box in torch 30-degree angled.....	89
Figure 8.19: T011, T012, T013, T014 Welding Beads.....	89
Figure 8.20: T015, T016, T017 Welding Beads	89

LIST OF TABLES

Table 3-1: Comparison of various WAAM techniques.[3]	25
Table 3-2: Effect on Bead Geometry [24,25]	27
Table 3-3: Effect on Heat Input and Bead Width [24,25]	27
Table 3-4: Impact on Material Properties and Defects [25]	28
Table 3-5: The 4 factors-3 levels design matrix.[26]	30
Table 3-6: Common Welding Defects in WAAM and their Causes	33
Table 3-7: Summary of Testing Methods in WAAM	37
Table 3-8: Comparative Summary of Welding Processes for WAAM	38
Table 3-9: A few examples of robotics in Additive Manufacturing. [33 - 36]	40
Table 3-10: Comparison of robotic systems that are suitable for this project [33 - 36]	41
Table 4-1: Gantry type Comparison	50

LIST OF ABBREVIATIONS

Abbreviation	Description
MAM	Metal Additive Manufacturing
AM	Additive Manufacturing
PBF	Powder Bed Fusion
SLM	Selective Laser Melting
EMB	Electron Beam Melting
MJ	Material Jetting
BJ	Binder Jetting
DED	Direct Energy Deposition
WAAM	Wire Arc Additive Manufacturing
MIG	Metal Inert Gas
CMT	Cold Metal Transfer
PAW	Plasma Arc Welding
WFR	Wire Feed Rate

1 INTRODUCTION

1.1 Background

Additive manufacturing (AM), commonly known as 3D printing, has transformed the landscape of modern manufacturing by enabling the layer-by-layer fabrication of complex geometries directly from digital models. While polymer-based 3D printing technologies have become mainstream, metal additive manufacturing remains a rapidly evolving field, with significant potential in aerospace, automotive, biomedical, and tooling industries. Among the various metal AM processes, Wire Arc Additive Manufacturing (WAAM) stands out due to its high deposition rates, cost-efficiency, and ability to produce large-scale metallic components using wire feedstock.

In WAAM, welding-based processes such as MIG (Metal Inert Gas) or TIG (Tungsten Inert Gas) welding are repurposed to deposit molten metal layer by layer. MIG welding, in particular, offers simplicity, affordability, and compatibility with various ferrous and non-ferrous metals, making it a suitable candidate for low-cost metal 3D printing systems.

1.2 Motivation

Despite the advantages of WAAM, its implementation is often limited by the high cost of commercial systems, limited accessibility in developing regions, and the lack of open-source, small-scale solutions. In Sri Lanka, the field of metal additive manufacturing is still in its infancy, with limited research and development initiatives. There is a critical need for an affordable, modular, and adaptable metal 3D printing system that can serve as a foundation for future research and industrial applications.

This project addresses this need by designing and developing a low-cost metal additive manufacturing system using MIG welding, integrated with a three-axis gantry robot system. The system is intended to offer a platform for experimenting with WAAM, exploring process parameters, and validating simulated results to advance understanding and adoption of this technology.

1.3 Scope of the Project

The project involves the design, development, and verification of a functional prototype metal additive manufacturing system from the combination of Gas Metal Arc Welding (GMAW) and a three-axis gantry robot. The system is to generate simple metallic parts by layer-by-layer deposition of mild steel wire. Research aims at developing an economical and low-cost WAAM solution, especially for SMEs and academia.

The work involves mechanical design and construction of the gantry, hardware integration of RETOP MIG-275 welding, firmware integration with Marlin and RAMPS 1.4, experimental verification through printing tests, and thermal simulation using ANSYS DED for thermal behaviour and residual stress computation. Weld parameters were analysed experimentally to enhance deposition quality.

The project scope doesn't encompass closed-loop control by weld bead monitoring, large-scale printing, post-deposition material characterization, and manufacture of complicated overhanging geometries. Nevertheless, the system effectively validates basic WAAM concepts and provides a foundation for further development in low-cost metal 3D printing.

1.4 Aim and Objectives

1.4.1 Aim

Design and development of a metal additive manufacturing system to fabricate complex components, which are hard to fabricate using conventional manufacturing processes

1.4.2 Objectives

- To identify metal additive manufacturing system parameters.
- To design and development of a metal additive manufacturing system to fabricate components.
- To automate the metal additive manufacturing system.
- To experimentally validate the developed system.

1.5 Structure of the Report

The report is organized into nine chapters to present holistically the design, development, and verification of an additive manufacturing system for metals based on Gas Metal Arc Welding (GMAW) combined with a gantry robot. Chapter 1 initiates the report, covering the background, motivation, objectives, scope, and general arrangement of the research. Chapter 2 is a detailed literature review of cutting-edge metal additive manufacturing technologies, namely Wire Arc Additive Manufacturing (WAAM), MIG welding processes, robot platforms based on a gantry, and associated control systems.

Chapter 3 presents the system design and development in the form of conceptual framework, mechanical setup, welding integration, electronics setup, and G-code flow. Chapter 4 explains the methodology adopted, detailing the setup fabrication, welding parameter optimization, ANSYS DED simulation studies, and control system development.

Chapter 5 gives the experimental test results, such as printing trial results, bead geometry analysis, cross-sectional observations, and simulation prediction comparisons. Chapter 6 deals with control system design, with a detailed discussion of the motion control implementation, torch activation, and the strategy developed for constant arc length maintenance through arc current feedback.

Chapter 7 finishes the report with an overview of the main discoveries, a quantification of the system performance, and suggestions for future development like real-time control and material testing after deposition. Chapter 8 gives a full list of references employed in the report in IEEE format. Chapter 9 has appendices with supporting materials like CAD models, sample G-code, firmware code, calibration outcomes, and circuit diagrams.

2 METHODOLOGY

1. Identify research gaps in metal additive manufacturing through a literature review using databases like Research Gate and IEEE Xplore. (Objective1)
2. Study MAM processes and parameters by analysing technical papers, patents, and industry reports. (Objective1)
3. Simulate the MAM process with software like ANSYS to predict and optimize system behaviour. (Objective2)
4. Manually create test pieces to validate simulations and identify issues using basic manufacturing techniques. (Objective2)
5. Detect defects and errors using material tests such as X-ray diffraction and tensile testing. (Objective2)
6. Choose a cost-effective manufacturing method to ensure accessibility for SMEs and research institutions. (Objective3)
7. Automate the manufacturing process by integrating PLCs and robotics for improved precision and repeatability. (Objective3)
8. Develop a manipulation structure to 3D metal print using the adapted metal manufacturing method. (Objective3)
9. Automate 3D printing operations using sensors and control systems to fabricate complex metal components. (Objective4)
10. Evaluate component quality by measuring accuracy, strength, and surface finish with equipment such as profilometers. (Objective4)
11. Compare simulations with test results using statistical analysis to refine and validate the models. (Objective4)

3 LITERATURE REVIEW

3.1 Additive Manufacturing Systems

Additive Manufacturing has rapidly emerged as one of the main drivers in the manufacturing industry because of its capability for complex geometries, reduced waste, and rapid prototyping. Unlike traditional subtractive manufacturing methods, AM is a process for building objects in layers from 3D model data [5]. The shift in technology has impressive implications for industries such as aerospace, automotive, and healthcare through the fabrication of complex, lightweight, and custom-designed components [6].

For example, AM has the potential not only to reduce lead times but also to significantly lower production costs, especially in small-series production or custom parts. The second advantage is that it allows material efficiency because waste can be minimized due to the use of only that amount of material which is required by the part. For example, the traditional fabrication of metal parts from large blocks of material can be as high as 90% wastage, whereas AM is able to achieve material utilization efficiencies of greater than 95% [7].

Hereafter, in this subsection, we will be reviewing the literature on metal additive manufacturing and other additive manufacturing systems such as powder bed fusion, material jetting, binder jetting, and direct energy deposition.

3.1.1 Metal Additive Manufacturing

Metal AM processes are generally categorized based on the type of feedstock used (powder or wire) and the energy source (for example laser, electron beam and arc). Such processes include the Powder Bed Fusion (PBF), Direct Energy Deposition (DED), Material Jetting (MJ) and Binder Jetting (BJ), all of which have advantages given the application. The development of AM is aiming at a more sustainable production method with lower carbon footprints and energy use, especially given that the material costs decline while process control is increasingly refined [7].

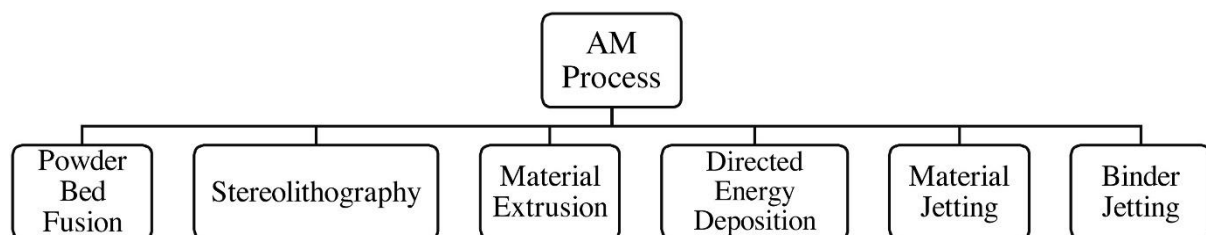


Figure 3.1: Additive Manufacturing Processes [6]

3.1.2 Powder Bed Fusion (PBF)

Powder Bed Fusion (PBF) is one of the most widely used techniques in metal additive manufacturing. As stated by R. Singh *et al*, this process, uses a heat source, typically a laser or electron beam, is used to selectively fuse regions of a metal powder bed layer by layer to form a part. PBF can be further categorized into methods like Selective Laser Melting (SLM) and Electron Beam Melting (EBM). SLM uses a laser to melt the powder, while EBM employs an electron beam to achieve the same goal [8].

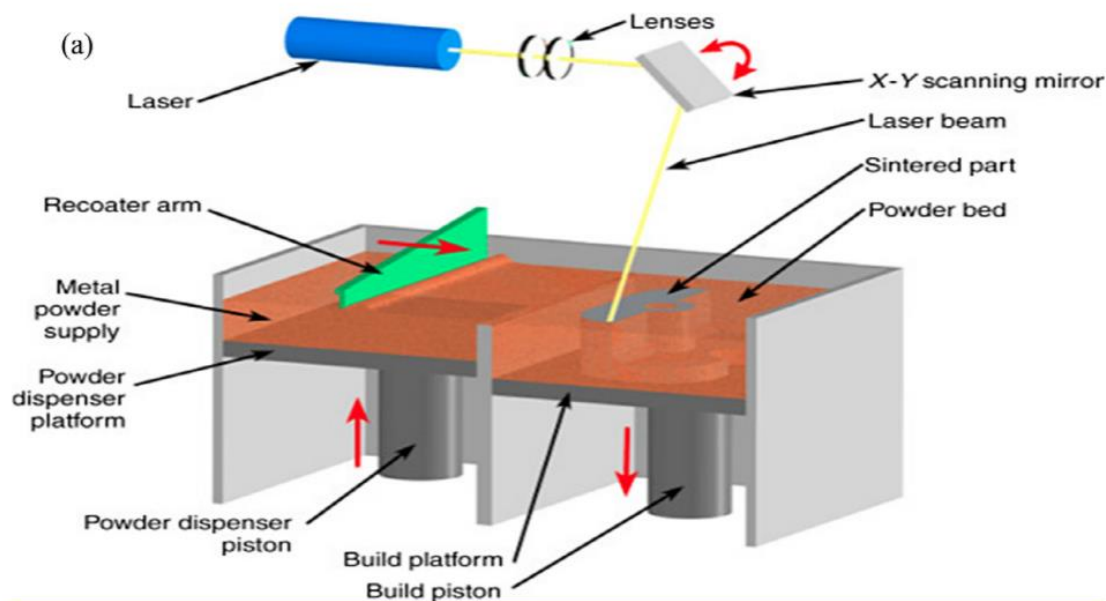


Figure 3.2: Powder Bed Fusion

3.1.3 Material Jetting (MJ)

Material Jetting (MJ) is another AM technique where droplets of material are selectively deposited and cured layer by layer to form a part. This method is commonly compared to inkjet printing but involves jetting materials like polymers, waxes, or even metals [10]. MJ is particularly advantageous for producing parts with high resolution and fine surface finishes. One of the key strengths of material jetting is its ability to print multi-material components, allowing for functionally graded materials and intricate designs to be fabricated in a single process [10].

3.1.4 Binder Jetting (BJ)

As shown by Ziaee *et al*, Binder Jetting (BJ) is a powder-based AM fabrication process which does not involve the use of heat to bond the particles of the powder bed material. Thus, instead

of using a solid binder it is sprayed in liquid form on to the powder bed to set the particles together. After the object is fully printed, it still in a green state, it needs other post-processing such as sintering, to acquire the final mechanical properties [9]. This remains one of the key strengths of BJ since it permits the formulation to be built rapidly and at the same time is compatible with a broad range of powdered materials such as metals, ceramics, and polymers[8] .

As mentioned above, BJ has various advantages such as flexibility and high production rate; however, it has difficulties such as a low mechanical strength of the green parts, and large post-treatment requirements. Obtaining high-density parts using sintering can be challenging since the process part shrinks and generates pores. In comparison to PBF, binder jetting is less accurate and the process steps to improve the surface quality and mechanical properties of the part have to be added[9].

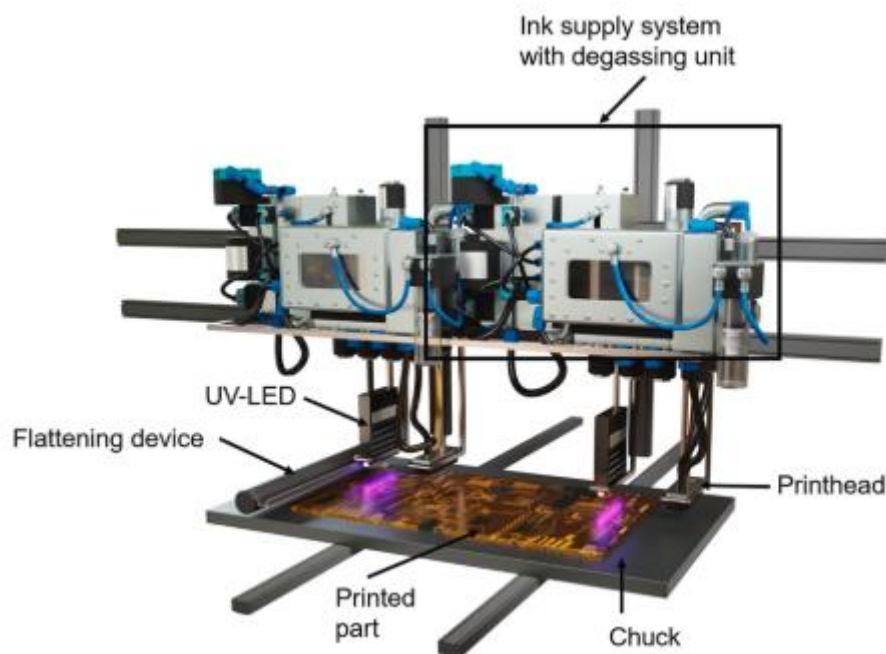


Figure 3.3: Binder Jetting

3.2 Direct Energy Deposition Methods (DED)

Direct Energy Deposition (DED) is a versatile additive manufacturing process that can use either powder or wire feedstock to build parts by fusing material with an energy source such as a laser, electron beam, or plasma arc. DED processes are often characterized by their ability to deposit material onto existing parts, making them ideal for part repair and refurbishment,

such as for worn-out or damaged components in critical industries like aerospace and heavy machinery.

DED systems work by delivering the material (either powder or wire) through a nozzle into a molten pool created by the energy source. The material solidifies as the nozzle moves across the substrate, building the part layer by layer. This process is repeated to create the desired shape. Unlike Powder Bed Fusion (PBF) systems, where the part is built within a bed of powder, DED can build directly onto existing surfaces, providing greater flexibility for part repair or augmentation.

DED processes are particularly advantageous for large structures, as they can achieve higher deposition rates compared to powder-based systems. For example, Optomec's Laser Engineered Net Shaping (LENS) system can achieve deposition rates in the range of several kilograms per hour, making it suitable for manufacturing and repair applications where large volumes of material are required [7]. However, one of the main challenges with DED systems is achieving fine surface finishes and maintaining dimensional accuracy. Post-processing, such as CNC machining, is often required to achieve final specifications.

3.2.1 Advantages of Direct Energy Deposition

There are multiple advantages of using DED in additive manufacturing.

- **High Deposition Rates** - DED systems can build parts quickly, making them suitable for large structures [11].
- **Repair and Refurbishment** - DED can deposit material on existing parts, extending their lifecycle and reducing the need for entirely new components. [12].
- **Flexible Feedstock Options** - Both powder and wire can be used in DED systems, depending on the application[12].
- **Large Build Volumes** - DED is well-suited for producing larger parts compared to Powder Bed Fusion (PBF) systems [13].

Despite these advantages, DED also faces some limitations. Achieving high surface quality can be challenging, and the process may introduce defects like porosity or inconsistent microstructures. Closed-loop control systems, real-time monitoring, and advanced sensors are critical to overcoming these issues and ensuring consistent quality [7]

3.2.2 Laser Metal Deposition (LMD)

Laser Metal Deposition (LMD) involves directing a laser beam onto a substrate while concurrently feeding metal powder or wire into the laser's path. The material melts and solidifies rapidly, creating a metallurgical bond with the substrate or previously deposited layers. This process can be automated and allows for precise control over material deposition, making it ideal for producing intricate geometries, complex shapes, and repairs of high-value components.[14]

3.2.3 Wire Arc Additive Manufacturing (WAAM)

Wire Arc Additive Manufacturing (WAAM) is a specific type of DED process that uses a metal wire as the feedstock and an electric arc as the energy source to melt and deposit material.[15] WAAM is particularly suited for fabricating large metal structures due to its high deposition rates and relatively low equipment cost compared to laser or electron beam-based systems. It shares many similarities with traditional welding processes like Gas Metal Arc Welding (GMAW), but it is optimized for the controlled deposition of material layer by layer to build up a part.[16]

WAAM systems typically use a gantry or robotic arm to move the deposition head across the build surface. As the wire is fed through the nozzle, an electric arc melts the wire, which solidifies upon cooling. This process can be repeated layer by layer to create components with high material utilization [7].

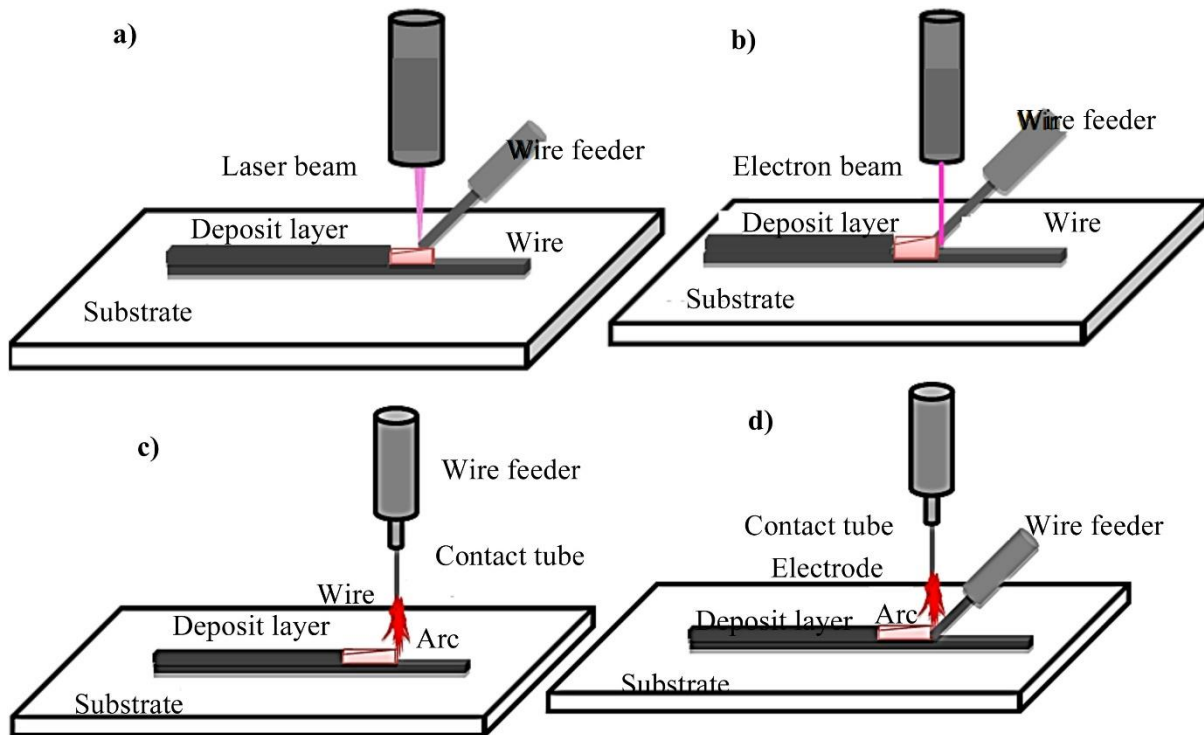


Figure 3.4: a) Wire Laser Additive Manufacturing (WLAM) b) Electron Beam Additive Manufacturing (EBAM) c), d) Wire Arc Additive Manufacturing (WAAM) [7]

3.2.3.1 Key Advantages of WAAM

- **High Deposition Rates** - WAAM offers some of the highest deposition rates among metal AM technologies, capable of depositing several kilograms of metal per hour. This makes it ideal for large-scale manufacturing, particularly in industries like aerospace, shipbuilding, and construction, where large metal parts are required.[11]
- **Cost-Effective** - WAAM is typically more affordable than powder-based systems due to the lower cost of wire feedstock and the use of more conventional welding equipment.[17]
- **Flexibility in Materials** - A wide range of materials can be used in WAAM, including steel, titanium, and aluminium alloys. This versatility makes WAAM a popular choice for industries that require strong, durable metal parts [1].
- **Repair Capabilities** - Like other DED processes, WAAM can be used for repair and refurbishment of components, making it a valuable tool for extending the lifespan of critical parts.

3.2.3.2 Limitations and Challenges

- **Surface Finish and Post-Processing** - WAAM generally produces rougher surfaces compared to powder-based AM methods, which often requires extensive post-processing, such as machining or grinding, to achieve the final surface finish and dimensional accuracy.[18]
- **Microstructural Control** - Managing the thermal history of the part during the WAAM process is critical to achieving desirable mechanical properties. Rapid cooling can introduce residual stresses, warping, or inconsistent microstructures. Researchers are exploring ways to control the cooling rates and improve the quality of WAAM-built parts [7].
- **Process Monitoring and Control** - WAAM systems require sophisticated monitoring and control systems to ensure consistent part quality. Real-time sensing of the melt pool, along with feedback control systems, is essential to mitigate defects like porosity, cracking, and inconsistent layer adhesion [7].

Overall, WAAM is a powerful tool for large-scale metal AM applications, particularly when high deposition rates are required. Its growing adoption in industries like aerospace, marine, and energy reflects its ability to produce large metal components more efficiently and cost-effectively compared to traditional methods[7]. Also, with higher deposition rates, flexibility in materials and higher repair capabilities WAAM is the most suitable AM process

3.3 Welding in WAAM Systems

3.3.1 Wire Arc Additive Manufacturing (WAAM)

Wire Arc Additive Manufacturing (WAAM) is a subcategory of metal additive manufacturing in which a wire is melted and deposited in a layer-by-layer method using an electric arc as the heat source [19]. Because of the high deposition rates and the potential to fabricate metallic components at scale with reduced costs than other metal additive manufacturing techniques such as powder bed fusion as the mentioned in section above, this process has garnered significant attention. Large, complex metal structures are needed in industries such as aerospace, automotive, and marine, making WAAM particularly attractive [20].

Welding processes used in WAAM are typically Gas Metal Arc Welding (GMAW), Gas Tungsten Arc Welding (GTAW), or Plasma Arc welding (PAW). Of these, GMAW, or MIG (Metal Inert Gas) welding, is widely favoured for its high deposition rate and the

straightforward compatibility with a variety of materials, including steel, aluminium and titanium alloys. Cold Metal Transfer (CMT) can also be integrated into advanced control techniques for MIG welding, which can better control the amount of heat input, thereby reducing defects such as porosity and cracking. [20].

Table 3-1: Comparison of various WAAM techniques.[3]

WAAM	Energy source	Features
GTAW-based	GTAW	Non-consumable electrode; Separate wire feed process; Typical deposition rate: 1-2 kg/hour; Wire and torch rotation are needed;
GMAW-based	GMAW	Consumable wire electrode; Typical deposition rate 3-4 kg/hour; Poor arc stability, spatter;
	Cold metal transfer (CMT)	Reciprocating consumable wire electrode; Typical deposition rate: 2-3 kg/hour; Low heat input process with zero spatter, high process tolerance;
	Tandem GMAW	Two consumable wires electrodes; Typical deposition: 6-8 kg/hour; Easy mixing to control composition for intermetallic materials manufacturing ;
PAW-based	Plasma	Non-consumable electrode; Separate wire feed process; Typical deposition rate 2-4 kg/hour; Wire and torch rotation are needed;

When compared to traditional manufacturing methods WAAM has the potential to reduce material waste and production costs. However, there are challenges to achieve the same part quality as repeatable residual stress, geometric accuracy, and defect formation. These issues are increasingly addressed by advanced control systems and process simulations in order to optimize WAAM processes for high quality manufacturing. [22], [23].

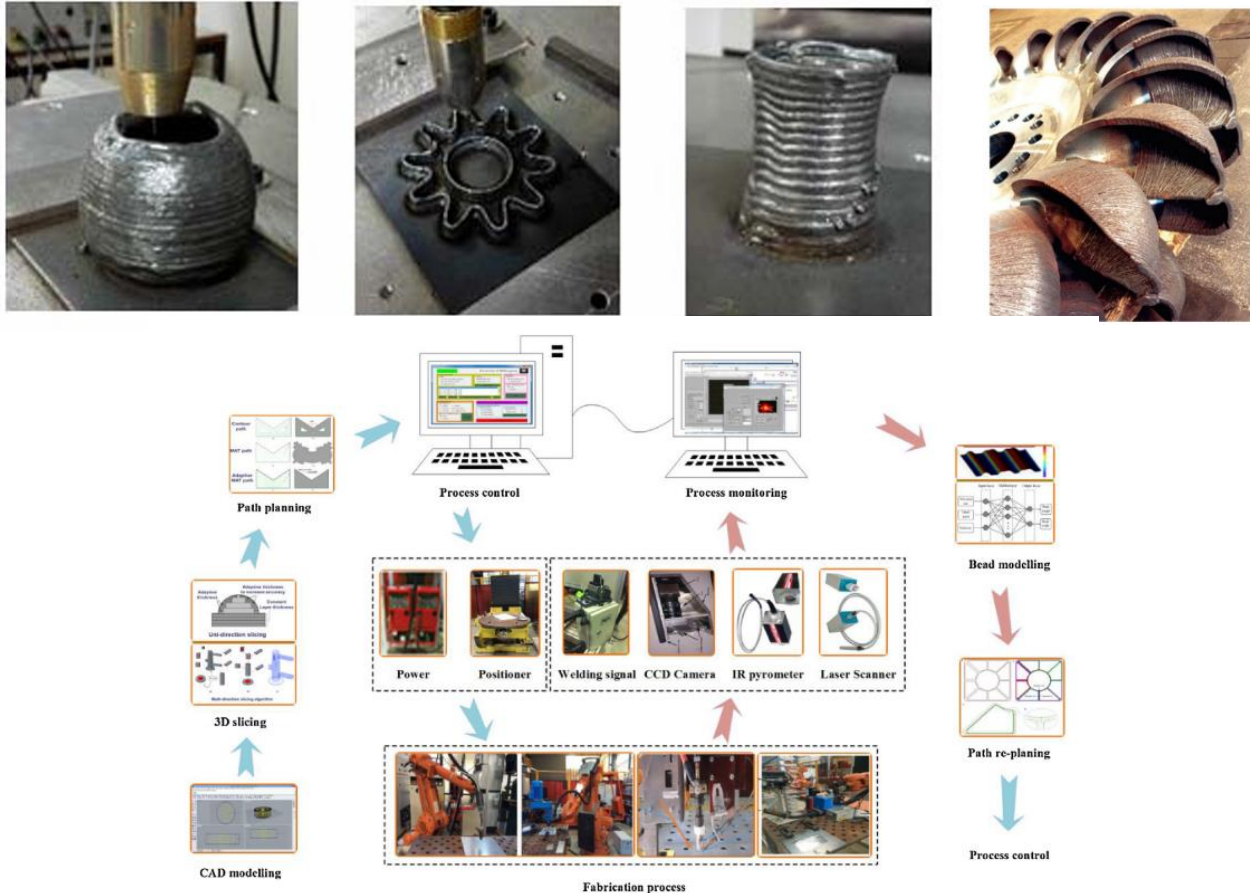


Figure 3.5: WAAM system design concepts, University of Wollongong.[3]

For this subsection, we will review the literature about welding parameters, welding defects, welding simulations, and welding testing methods. Finally, we will be comparing all WAAM welding processes for a better comparison.

3.3.2 Welding Parameters in WAAM

Wire Arc Additive Manufacturing (WAAM) is highly sensitive to several key process parameters that directly impact the deposition quality, material properties and the overall mechanical integrity of the fabricated component. Achieving consistent and defect free production requires understanding and optimizing these parameters. In this section, the general welding parameters in WAAM such as travel speed, wire feed rate, current, voltage and heat input are defined.

3.3.2.1 Wire Feed Rate

Among the most important factors in WAAM is the wire feed rate, which directly controls deposition rate and bead geometry. This leads to a taller and narrower weld bead if the material deposition is increased with higher wire feed rate [24]. But if the feed rate is too high, too much build up in the material and defects like lack of fusion or excessive porosity can occur. In contrast, if the wire feed rate is too low, then the bead may not be properly formed especially for multi-layer builds [25]. The optimal wire feed rate must be balanced in practice in order to achieve proper material deposition and uniform bead characteristics.

Table 3-2: Effect on Bead Geometry [24,25]

Parameter	Effect on Bead Geometry
Low Feed Rate	Narrower, less material deposited
High Feed Rate	Taller, more material deposited, potential defects

3.3.2.2 Travel Speed

The bead's width, height and roughness are directly influenced by the travel speed (or speed at which the welding torch moves along the deposition path). The slower travel speed allows more heat to be introduced in the material and increase the bead width and improve fusion between the layers [24], [25] but at the expense of undesirable results like excessive distortion or residual stress buildup. Instead, heat input is reduced with high travel speeds, leading to narrower beads and poorer fusion quality. Thus, the optimal travel speeds should be chosen for a particular material to balance heat input and bead geometry.

Table 3-3: Effect on Heat Input and Bead Width [24,25]

Parameter	Effect on Heat Input and Bead Width
Low Travel Speed	Higher heat input, wider bead
High Travel Speed	Lower heat input, narrower bead

3.3.2.3 Current and Voltage

The energy input into the process is controlled by current and voltage in WAAM, and this energy input directly influences the size of the weld pool, penetration depth and overall heat distribution. Generally, higher current settings increase the heat input, and thus deeper penetration and wider beads [24]. But as the current increases, so does the risk of defect generation, namely undercutting and spatter. However, low current settings may not produce enough fusion and poor bead integrity. The current and the voltage are adjusted side by side to affect arc stability and bead smoothness. The arc can be spatter at lower voltages, but higher voltages result in a more stable arc but with an increased risk of excessive bead spreading [25].

3.3.2.4 Heat Input

A number of interrelated parameters, such as current, voltage and travel speed, are dependent on heat input. And it determines the thermal cycle that the material sees, both in terms of cooling rate and residual stresses and its microstructure. Controlling heat input is a critical factor in managing distortion, reducing residual stress and obtaining desirable properties in WAAM. For example, in high strength structural steels it is important to control heat input to avoid excessive softening of the material and maintain high tensile strength [25].

Table 3-4: Impact on Material Properties and Defects [25]

Heat Input	Impact on Material Properties and Defects
High Heat Input	Increased risk of distortion, wider beads, slower cooling, lower tensile strength
Low Heat Input	Faster cooling, potential for cracking due to high stress gradients, finer microstructure

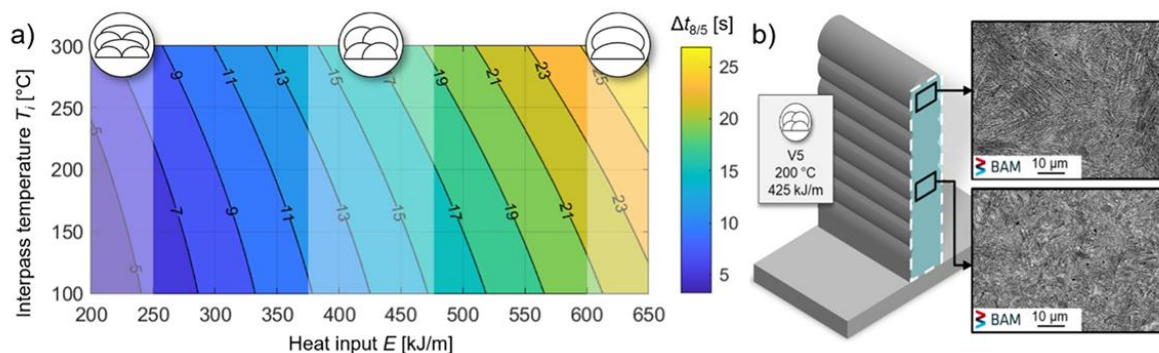


Figure 3.6: a) Contour plot of cooling time $\Delta t_{8/5}$ as a function of heat input E and interlayer temperature T_i (quadratic regression model, model quality $R.2 = 98.6\%$); b) SEM images of the microstructures for two regions of the wall cross section of WAAM specimen V5 [25]

3.3.2.5 Interlayer Cooling

Temperature between successive layers is also critically important in WAAM. When interlayer cooling is not enough, the last component can experience excessive heat accumulation, which can result in thermal distortion and the formation of unwanted microstructures, such as coarse grains, which weaken the final component. The cooling times ($\Delta t_{8/5}$) between 800°C and 500°C are monitored and controlled to optimize heat dissipation and mechanical strength [24]. Larger grain sizes and reduced strength of the material are a consequence of slower cooling rates, which are more often the case when the heat input is high.

3.3.2.6 Shielding Gas Flow

Shielding gas (usually argon) plays a key role in protecting the molten weld pool from oxidation, and other atmospheric contaminants, as it is being formed during the WAAM process. An insufficient flow rate of the shielding gas will result in oxidation and porosity of the weld bead [24]. However, if too much gas flow, the weld pool can become turbulent and disturb the deposition process. The size and material of the weld bead dictates what the optimal gas flow should be to create a stable and clean environment for deposition.

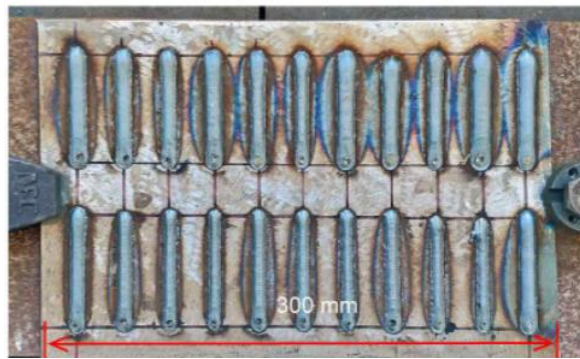
Finally, the conclusion is that each of these parameters has a major impact on the quality of a WAAM process. In order to minimize defects and achieve desired mechanical properties in the final component, it is important to find the optimal combination of these parameters. In many cases, it is necessary to run multiple experimental runs and employ simulation tools to better tune these parameters according to specific materials and part geometries [24], [25].

Hu, Zeqi et al. [8] experimented at Wuhan University of Technology. The experiment follows a full-factorial design with four key welding parameters: Arc voltage (AV), torch travel speed (TTS), contact tip to workpiece distance (CTWD), and wire feed speed (WFS). A non-contact 3D laser scanner is used to measure the geometrical features of the welding bead: width, height, and cross-sectional area. A weld bead geometry prediction is made using an ANN model based on welding parameters. These geometrical features are then used by a backward prediction model (FANN-GA) to determine the optimal welding parameters.

Table 3-5: The 4 factors-3 levels design matrix.[26]

Level	WFS(m/min)	AV(V)	TTS(mm/s)	CTWD(mm)
1	3.5	21.6	4.0	8.0
2	5.0	22.2	6.0	13.0
3	6..5	23.0	8.0	18.0

A six-axis ABB IRB 1410 robot and GMAW equipment were used in the experimental setup to perform single layer and multi-layer depositions and the accuracy of the proposed method's predictions of parameters and the bead geometry were validated.

*Figure 3.7: Part of the actual weld bead in the experiment.[26]*

3.3.3 Welding Defects in WAAM

The Wire Arc Additive Manufacturing (WAAM) process commonly express welding defects that can have a significant impact to the mechanical properties, integrity and the quality of the produced parts. The defects can be from an improper process control, environmental factors, and the material that is being used. In this section we discuss the principal defects occurring in WAAM, namely cracking, porosity, lack of fusion and geometric distortions.

3.3.3.1 Porosity

The most common defect in WAAM is porosity with gas-filled voids within the material. Contamination of the feedstock or substrate, absorption of moisture, or incorrect flow of shielding gas may lead to the formation of these voids. Due to the impact of mechanical properties, for example, tensile strength, in WAAM parts the mechanical properties are affected by porosity negatively, with reduced tensile strength and a higher probability of fatigue failure [27], [28].

There are two main types of porosity.

- **Material-induced porosity:** This occurs when impurities such as moisture or hydrocarbons present on the feedstock wire or substrate are trapped in the weld pool. Upon cooling, gases can be released, forming spherical or irregular voids.
- **Process-induced porosity:** This arises from unstable process parameters, such as improper wire feed speed, travel speed, or welding current, leading to insufficient fusion and the creation of voids within the weld [27].

To mitigate porosity, clean feedstock is used, shielding gas flow is optimized, along with advanced techniques such as Cold Metal Transfer (CMT) to reduce heat input and stabilize the weld pool [8].

3.3.3.2 Cracking

Another critical defect for WAAM is cracking, which often occurs during or after solidification as a result of thermal stresses. Cracks can be categorized as:

- **Hot Cracks:** They are produced during solidification when different parts of the weld pool cool at different rates resulting in high internal stresses. Solidification cracks, also called hot cracks, generally occur along the grain boundaries and can weaken the component in its entirety.
- **Cold Cracks:** These are formed when the residual stress in the material exceeds the material tensile strength during solidification. Cold cracks often [27], [28] occur in low temperature or insufficient preheating.

The cooling rate, composition of the welding wire and preheating the substrate, if required, may be used to minimize cracking [27].

3.3.3.3 Lack of Fusion

This occurs if successive layers or the neighbouring beads do not join sufficiently because of insufficient heat input or poor process parameters. The defect takes the form of small voids or complete separation between layers, resulting in a loss of structural integrity of the final component. For example, these travel speeds are thought to be inadequate, wire positioning is poor, or current is insufficient [28].

As with any process, the more we can reduce the occurrence of lack of fusion, the more we can ensure optimal heat input, and the more we are able to control current, travel speed and wire

feed rate. Process simulations can also predict areas where fusion may not be adequate and can provide data to change process parameters in real-time [27].

3.3.3.4 Geometric Distortions

Geometric distortions of WAAM, such as warping, bending, and buckling, are susceptible to high thermal gradients and repeated heating and cooling cycles in the process. The main causes of these distortions are mainly from residual stress that accumulates in the material as it cools unevenly. This issue is particularly problematic for large thin-walled structures [28].

Proper path planning, interlayer cooling, and in some cases mechanical or thermal post processing such as interpass rolling or stress relief annealing [27] can be used to minimize distortion.

3.3.3.5 Oxidation and Surface Contamination

When the molten weld pool is exposed to oxygen or moisture in the atmosphere, it oxidizes, and it begins to surface contaminate. Oxides that form on the surface may result from inadequate shielding gas flow or an insufficiently controlled welding environment and can produce weak joints or poor layer adhesion. Welding of reactive materials such as titanium is problematic due to the high reactivity of the material with oxygen [27], [28].

Prevention of oxidation and surface contamination is critical and depends on maintaining a controlled atmosphere, using high purity shielding gases and ensuring proper sealing of the welding chamber [28].

Table 3-6: Common Welding Defects in WAAM and their Causes

Defect	Cause	Impact	Mitigation
Porosity	Contaminated feedstock, improper shielding gas	Reduced tensile strength, fatigue failure	Clean feedstock, optimize gas flow, use CMT techniques
Hot Cracks	Differential cooling rates	Compromised structural integrity	Control cooling rate, optimize wire composition
Cold Cracks	Residual stress, low-temperature environment	Part failure	Preheating, post-process heat treatment
Lack of Fusion	Insufficient heat input, improper wire positioning	Weak joints, voids between layers	Adjust heat input, control travel speed and wire feed
Distortion	Residual stress from thermal cycling	Warping, buckling	Path planning, stress-relief annealing
Oxidation	Inadequate shielding gas, exposure to atmosphere	Weak joints, surface defects	Use high-purity gas, control welding environment

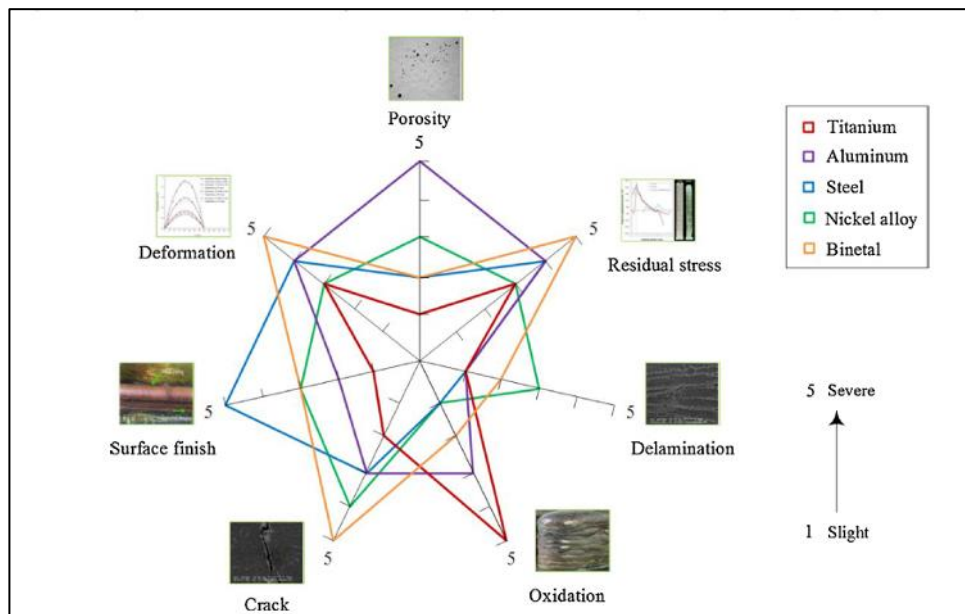


Figure 3.8: The correlation between materials and defects in WAAM processes. [28]

3.3.4 Welding Simulations in WAAM

Thermal behaviour, distortion, residual stress, and overall mechanical properties are predicted by welding simulations in Wire Arc Additive Manufacturing (WAAM). By using these simulations, process optimization is possible, which gives better control of defects and better quality of finished components. This section describes key aspects of welding simulating in WAAM using thermodynamics mechanical models and how they affect predicting outcomes such as heat distribution, residual stresses and distortion.

3.3.4.1 Thermal Simulations

In WAAM, thermal simulations are important because they predict heat transfer during the welding process and thereby affect the cooling rates, bead shape, and residual stresses in deposited layers. These predictions are important because their accuracy directly affects the material properties (hardness and tensile strength) of the fabricated part.

Temperature distribution in the weld pool and surrounding areas are calculated in most WAAM simulations using finite element (FE) models. The transient and steady-state thermal models are the two primary approaches for simulating thermal behaviour:

- **Transient Thermal Models:** These models monitor the movement of the heat source with time and give detailed temperature histories at selected time points during the deposition process. The simulations are highly accurate but computationally intensive [29].
- **Steady-State Thermal Models:** On the other hand, steady state models assume a final thermal state and reduces the simulation process and dramatically reduces computational time [29].

Steady state thermal models can reduce simulation time by approximately 80 per cent compared to transient models and therefore are a more efficient approach for large scale or multi-layer WAAM processes [29].

3.3.4.2 Mechanical Simulations

Residual stresses and distortions caused by thermally induced cycles in WAAM are predicted by mechanical simulations. Welding at high heat input can expand and contract the material leading to stress and part deformation.

- **Thermo-Mechanical Models:** These models are thermal and mechanical behaviour analysis combined to provide accurate predictions of residual stress development and distortion. The element birth and death method is widely used in mechanical simulations, where the material is added layer by layer as the process progresses.[29]
- **Residual Stress and Distortion Prediction:** Residual stress and distortions are predicted using finite element methods (FEM), and insights are gained into areas that require stress relief treatments. Stress levels are often highest near the weld bead, where during cooling large amounts of material contract [30]. These stresses redistribute after unclamping; they deform the part.

Post process heat treatments may be necessary in cases where high residual stress is predicted, to relieve stress and improve mechanical properties of the component [29], [30].

3.3.4.3 Validation of Simulation Models

Experimental data such as neutron diffraction strain measurements or thermocouple temperature measurements are compared to simulation results to validate the simulation models. For instance, in another case, thermocouple data obtained at multiple points on the base plate is used to validate thermal simulations, which show that transient and steady state models can accurately predict temperature distribution [29].

Similarly, mechanical simulations have been validated with experiment through comparison of predicted residual stresses and distortion with experimental measurements. Stress distribution within WAAM components has been verified using neutron diffraction [30], and the models are shown to be consistent with actual measurements.

3.3.5 Welding Testing Methods in WAAM

Wire Arc Additive Manufacturing (WAAM) requires testing methods to ensure the integrity and reliability of components produced. The mechanical properties, microstructural features, and defect characteristics of WAAM parts are evaluated using various testing methods, both destructive and non-destructive. In this section, the key testing methods utilized to evaluate WAAM components, including tensile testing, hardness testing, microstructural analysis, and non-destructive testing (NDT) are explored.

3.3.6 Tensile Testing

Destructive testing of WAAM components is normally performed using tensile testing, one of the most widely used methods of mechanical properties evaluation. Properties such as yield strength, ultimate tensile strength, and elongation at break are measured. For instance, mechanical properties of such materials are usually evaluated in tensile specimens extracted from various orientations, e.g. longitudinal and transverse directions in relation to the print layers, in WAAM [13]. ASTM or ISO standard tensile test setup was followed with stress-strained data being used to evaluate the key material properties.

A significant finding of WAAM of steel is that slower cooling rates associated with WAAM typically yield lower strength than conventionally produced steels. Nevertheless, WAAM components demonstrate good ductility and similar Young's modulus values [31]. In some cases, techniques as advanced as digital image correlation (DIC) are used to measure strain distribution across the specimen surface during testing, useful for identifying localized deformations and failure mechanism.

3.3.6.1 Hardness Testing

Evaluation of surface properties and wear resistance of WAAM components requires hardness testing. It consists of applying a controlled load on a hard indenter into the material surface and measuring the indentation size. The common methods include Rockwell, Vickers, or Brinell hardness tests, depending on the material being tested and the requirements of the application.

Hardness measurements of WAAM produced components are typically not uniform across different layers and regions due to the non-uniform thermal history present during deposition. In high strength steels [31], [32], hardness usually increases with regions where the cooling rates were higher, and which leads to finer microstructures such as martensite or bainite.

3.3.6.2 Microstructural Analysis

In WAAM components, microstructural analysis is performed to identify grain structure, phase composition, and defect distribution. For this purpose, techniques such as optical microscopy (OM), scanning electron microscopy (SEM), and electron backscatter diffraction (EBSD) are often used. By analysing these methods, they reveal insights into the anisotropy and crystallographic texture of WAAM materials and can directly impact their mechanical properties.

For example, produced by WAAM, high strength steel has a mixed microstructure of ferrite, bainite and martensite. Similarly, microstructural analysis can also explain why some WAAM materials exhibit isotropic mechanical behaviour despite the layered nature of the deposition process [31].

3.3.7 Non-Destructive Testing (NDT)

The testing of internal defects, such as porosity, cracks or lack of fusion, with non-destructive testing (NDT) methods is indispensable without damaging the component. The common NDT techniques in WAAM are.:

- **Ultrasonic Testing (UT):** Internal flaws are detected using ultrasonic waves, which are transmitted through the material. UT is particularly favourable for the identification of volumetric defects, for example, voids and cracks.
- **X-ray and Computed Tomography (CT):** High resolution 3D imaging of internal features is provided by these imaging techniques. WAAM is increasingly used for CT scanning of defects and internal structure of complex components in WAAM [14].
- **Dye Penetrant and Magnetic Particle Testing (MT):** In this work, these surface level tests are used to identify cracks and surface defects in ferrous materials such as those fabricated by WAAM [32].

Table 3-7: Summary of Testing Methods in WAAM

Testing Method	Purpose	Common Tools/Standards	Output
Tensile Testing	Evaluate mechanical properties (strength, ductility)	Universal Testing Machine, ASTM E8	Yield strength, ultimate tensile strength, elongation
Hardness Testing	Measure surface hardness and wear resistance	Vickers, Rockwell, Brinell hardness testers	Hardness values across layers
Microstructural Analysis	Analyze grain structure and phase composition	Optical Microscopy, SEM, EBSD	Microstructure details (ferrite, bainite, martensite)
Non-Destructive Testing	Detect internal defects (porosity, cracks)	Ultrasonic Testing, CT Scanning, X-ray	Defect location and size

3.4 Comparison Between Welding Methods.

MIG vs. TIG Welding: TIG welding, while providing excellent control over heat input and producing high-quality welds with minimal defects, has a significantly lower deposition rate than MIG. This makes TIG unsuitable for large-scale WAAM applications where build speed is crucial. Additionally, TIG welding equipment is more expensive to operate, particularly for large components.

MIG vs. Plasma Arc Welding (PAW): PAW offers good precision and can be used for WAAM, but it generally has a lower deposition rate than MIG. The complexity of PAW systems and the need for more advanced control mechanisms make MIG a more cost-effective and simpler option for most WAAM applications.

MIG vs. Laser/Electron Beam Welding: Laser and electron beam welding provide the highest precision and are often used in industries requiring tight tolerances, such as aerospace. However, the high costs associated with these technologies make them less accessible for general WAAM applications. MIG welding offers a balance of good precision, high deposition rates, and lower costs, making it more suitable for applications where cost-efficiency is important.

Table 3-8: Comparative Summary of Welding Processes for WAAM

Parameter	MIG Welding	TIG Welding	PAW
Deposition Rate	High	Low	Moderate
Cost	Low	High	Moderate
Heat Input Control	Good (with CMT)	Excellent	Good
Material Compatibility	High	Limited	Moderate
Precision	Moderate	High	High
Defect Rate	Low (with CMT)	Very Low	Low

3.5 Automating the System with Robot Systems

The following subsection reviews literature on automation technologies applied in AM and welding robotics with emphasis on the use of robots, and control systems. These literature reviews provided vital information for our final year project, which entails building a metal additive manufacturing system. The finding of the previous researchers pinpoints the improvement achieved in robot-integrated AM systems, particularly in WAAM, gantry, and robotic arm systems.

3.1 Overview of Robotic Systems in Additive Manufacturing (AM)

Additive manufacturing employs other types of robotic systems where accurate precision is required. The most common methods are,

- **Articulated Robot Systems:** These give relatively higher flexibility because of the multiple DOF values that range from 6 to above. These systems are employed for massive additive manufacturing applications that necessitate access to the printed part in one or multiple directions. The main disadvantage is that they are costlier and less stable than fixed systems. Also, the limitation is always in precise control of the deposition path, since the mechanical trajectories could be more complex [33, 34].

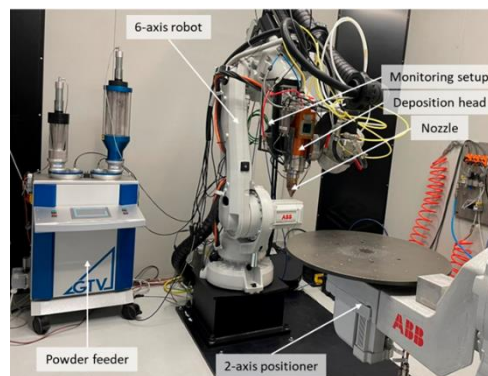


Figure 3.9: 8 Axis articulated robot [35]

- **Cartesian Systems:** These systems use fewer degrees of freedom (3-5 DOF) and offer higher precision and stability compared to articulated systems. Although they are limited in terms of flexibility, gantries provide an ideal balance between cost and ease

of use for large-scale and planar metal additive manufacturing [35]. Lan J *et al* [36] have used a cartesian system for the multi-material 3D printer.

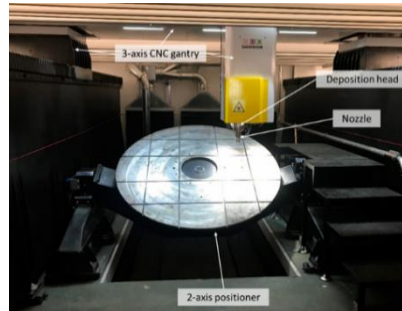


Figure 3.10 :5 DOF gantry robot system [3].

Robotics are mostly used in additive manufacturing, some examples of them are given in Table 8.

Table 3-9: A few examples of robotics in Additive Manufacturing. [33 - 36]

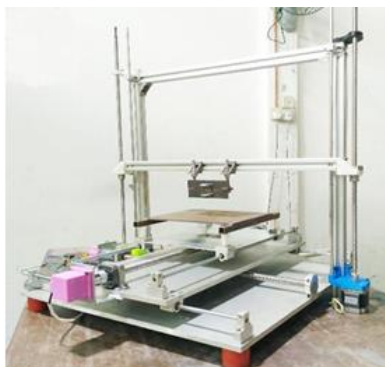
Robot and extruder type	DOF	Objective
ABB robot and a custom-designed fused deposition modeling (FDM) extruder	6	Development of collision-free trajectory planning for robot-based printing using a non-planar deposition [37].
Motoman model SV3X robot and a 0.4 mm extended nozzle with air-forced cooling system	6	performing multi-plane toolpath motions for 3D lattice structure parts printing [38].
ABB robot and a custom-designed fused deposition modeling (FDM) extruder	6	Tool path generation for non-planar Layers[39].
Custom five-axis AM setup	6	Optimization of the workpiece properties by changing the orientation of the extruded filament based on external loads and surface quality requirements and minimization of support material [40].
UR3 robotic arm and FDM extruder	6	Development of a new algorithm for decomposing models into support-free parts that can be printed one by one in a collision-free sequence [41].
KUKA robot and FDM extruder	6	Development of a new decomposition-based curved surface slicing and transformation-based cylinder surface slicing methods for toolpath generation [42].

Table 3-10: Comparison of robotic systems that are suitable for this project [33 - 36]

Robot System	Accuracy	Cost	Complexity	Speed
Gantry System	High precision	Cost-effective,	Low	Moderate
Articulated Arm	High accuracy	Expensive	High	Moderate to low
Delta Robot	High precision	Moderate	High	High speed

According to the above Table 9, the Gantry System has advantages compared to the other robot systems.

- **Cost-effectiveness:** Gantry systems are significantly cheaper than articulated robots, making them ideal for projects with budget constraints [35], [43].
- **Ease of Use:** Gantry robots' simpler control systems make them easier to program and maintain, requiring less specialized knowledge [43], [44].
- **High Precision:** For metal additive manufacturing, precision is paramount. Gantry systems, particularly those with micro stepper motors, provide excellent accuracy [43].

*Figure 3.11: low-cost metal 3D printer [45]*

3.2 Automation of the Welding Plant

For the welding machine part of this system, the critical parameters to automate will be discussed here onwards.

3.2.1 Current and Voltage Control:

These are typically regulated using microcontrollers or programmable logic controllers (PLCs) integrated with the welding machine's control systems [45].

3.2.2 Wire Feed Rate:

The feed rate can be controlled using precision stepper or servo motors, depending on the requirement for control accuracy. Microcontrollers allow for easy programming of different feed rates based on the geometry and requirements of the printed part [34], [43].

Dominic Cuiuri *et al.*[46] have modified the wire feed rate of a GMAW machine. The speed control system had a conventional structure of an inner current loop to control the torque output of the DC drive motor and an outer speed loop whose feedback was derived from a 500 pulse per revolution encoder mounted on the motor armature.

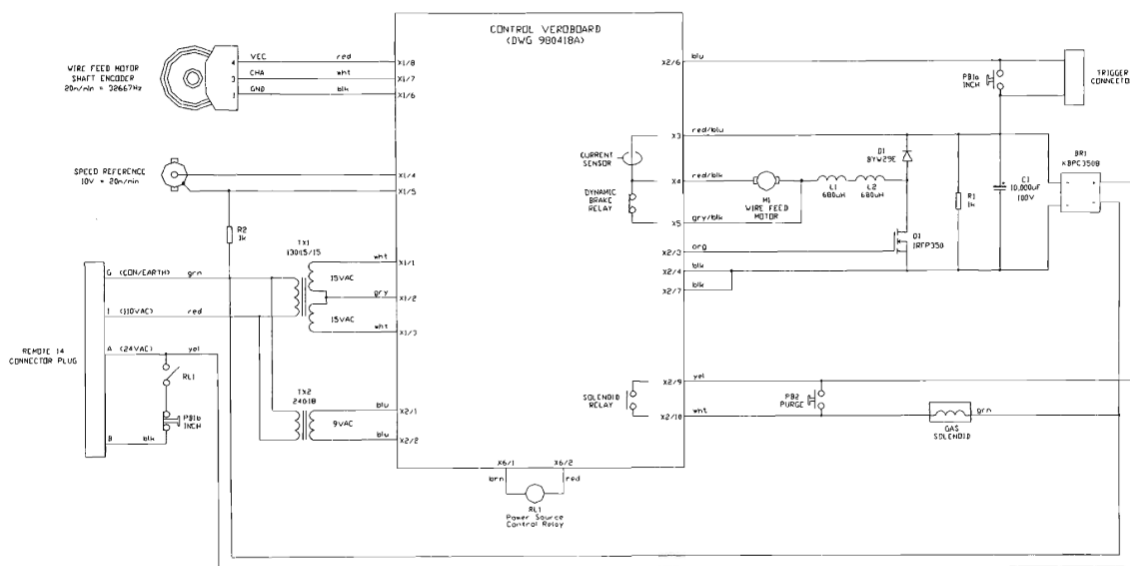


Figure 3.12: Wire feed unit main circuit schematic [46].

3.2.3 Arc Length Control in the Welding Machine

Particularly in the welding machines arc length control plays a very vital role in producing perfect and quality welds. As the automation of welding processes and particularly additive manufacturing progresses, keeping the arc length constant becomes critical to establishing similar deposition of metal layers.

N. A. Rosli *et al*, [47], in their work, didn't apply any arc length controlling method. They positioned the welding torch under the fixture design in the perpendicular direction to the bed to construct the surface. They have made 5 specimens, and all the tests did not give the correct dimension to the tolerance of (+/-) 0.5mm.

3.2.3.1 Categories of Arc Length Control Methods

Contact Sensors

- **Wire Touch Sensors:** These sensors find the position of the workpiece by passing a feeble current through the welding wire until it meets the base material. Upon contact, it informs the arc length and controls welding parameters correspondingly [47].
- **Contact Probe Sensors:** A probe attached to the welding torch allows the determination of the workpiece surface outline and thus the arc length [47].

Non-Contact Sensors

- **Arc Sensors:** These real-time arc sensors regulate the welding current, depending on the change in arc current. The position of the torch is varied depending on the current to obtain a constant arc length [47].

Pinar *et al*. [16] were researched about open-source voltage and current monitors for GMAW using an Arduino Uno. In their works, Miller Matic 140 and 190 MIG welding machines were used while doing adjustments to the machines for measuring current and voltage. The current transducer was used for current sensing and the circuitry was based on LM741. The voltage circuitry was based on AD629. Those were based on Integrated circuit amplifiers. Zener diodes were used for protection and the voltage dividers and smoothing decoupling capacitors were used as other components in the circuit.

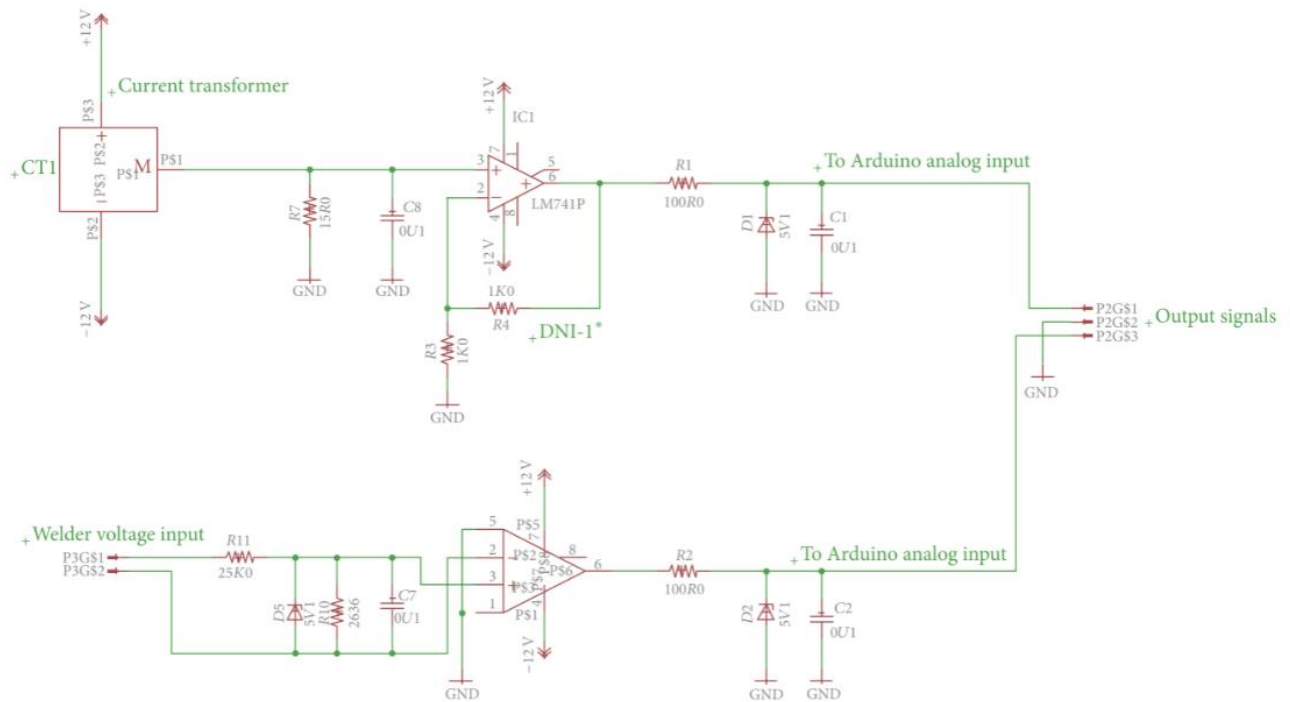


Figure 3.13: Current and voltage sensing circuitry [48].

- Laser Displacement Sensors:** Laser-based systems employ a laser sensor to determine the position of the welding torch relative to the workpiece without touching it. These sensors afford real-time arc length measurements with the high speeds and accuracies necessary for feedback control in fully automated welding operations [47].

Sakari Penttilä *et al.* [49] they studied the Artificial Intelligence-Enabled Feedback Control System in Robotized Gas Metal Arc Welding. In their work, they have used a Meta Vision SLS50-v1 laser triangulation sensor to measure the distance between the welding groove and the device.



Figure 3.14 Experimental setup with a close-up image of the torch configuration consisting of thermal sensor, welding torch and laser triangulation [48].

In the context of this project involving welding for additive manufacturing, arc and laser sensors offer superior advantages in terms of precision, and real-time feedback compared to other methods. The cost of laser sensors is higher compared to the other sensors [45].

3.3 Control Systems, Firmware, and Actuators

In gantry robot systems, controllers such as G-code interpreters are normally used for motion control and open-source firmware.

As previously mentioned, N. A. Rosli *et al.* [45] have used an Arduino MEGA 2560 as the control system and Cura open-source firmware. Nema 23 stepper motors, stepper driver 8825, ball screws, mild steel squares...etc. were used as the actuators and other components.



Figure 3.15 The mounted circuit to the welding machine [48].

Lan J *et al.* [36] have used an open loop mode for control positioning and linear guides, stepper motors, wire carriers, and timing belts as the components of their robot system.

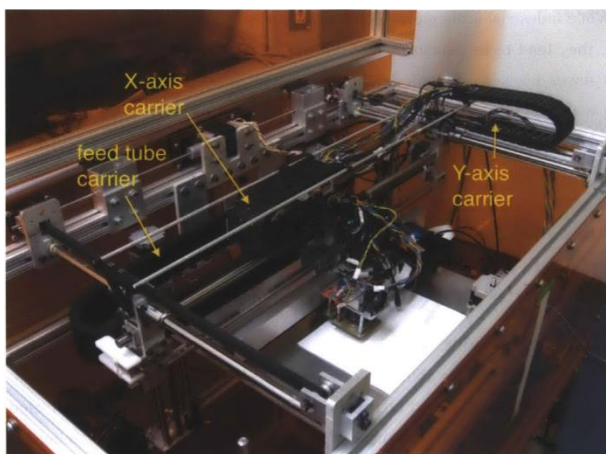


Figure 3.16 Components of the robot system [36]

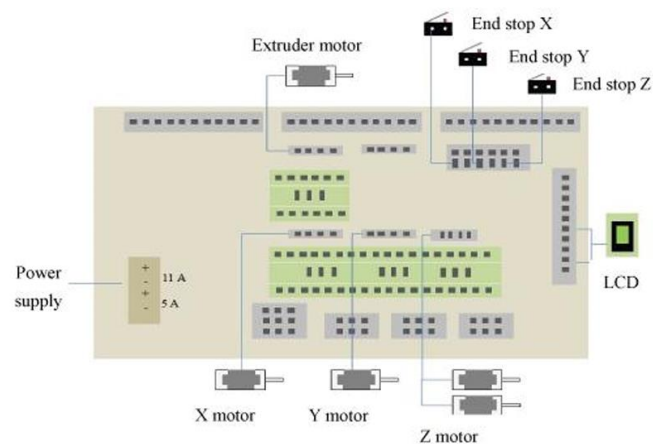


Figure 3.17 Connections of Arduino 2560 [36].

L. Stamorean *et al.* [39] developed a robot arm system for additive manufacturing applications. They have used an Arduino Mega 2560 with a Ramps 1.4 extruder driver board and Nema 17 stepper motor with a micro stepper controller.

Previously mentioned by Lan J *et al.* [36] used scaled precomputed ramps for input shaping. It has produced significantly fewer overshoots and fewer oscillations.

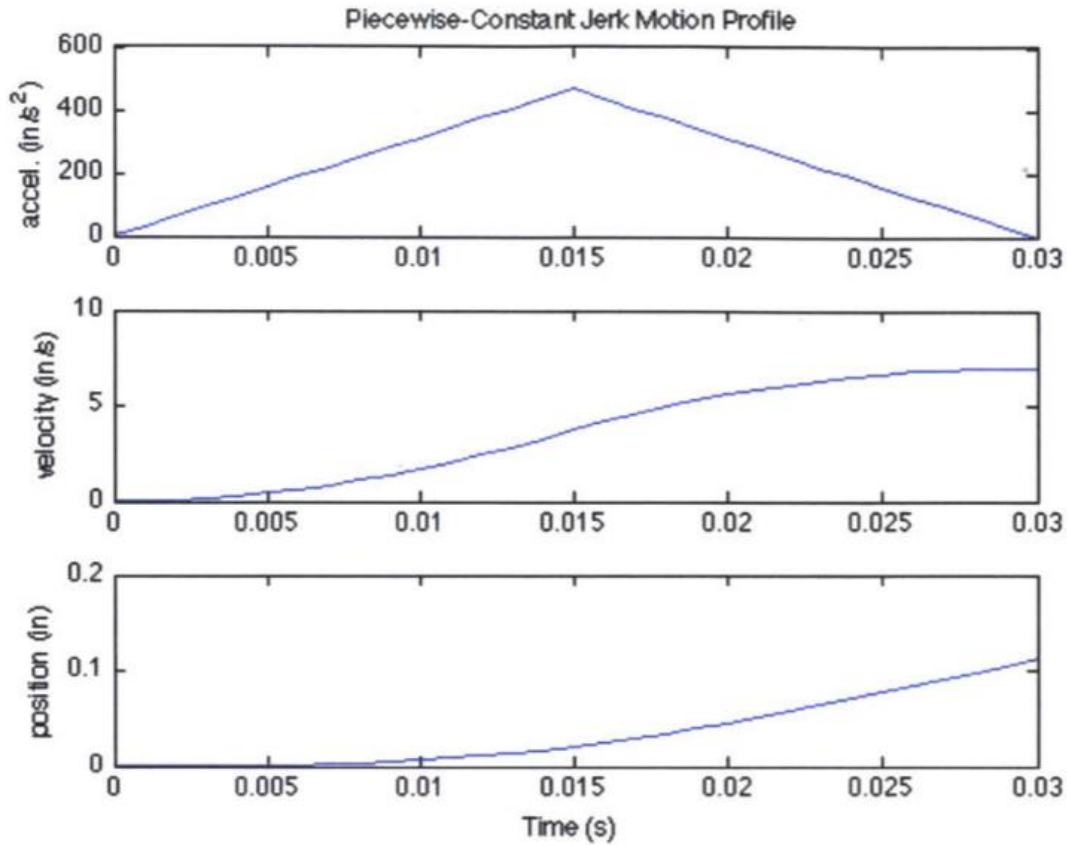


Figure 3.18: Acceleration, velocity, and position as a function of time using a piecewise-constant jerk profile, which linearly increases the system's acceleration to a maximum value then decreases it again [36].

The X-axis motor was tested at 15,000 micro steps per second, and acceleration was measured at 1065.8 in/s². This value was halved to 106 steps per square second for a conservative estimate used in trajectory calculations, while the carriage motion was measured with an encoder. Then using a quadratic polynomial, the maximum acceleration was taken as $1 \times 10^6 \mu\text{steps/s}^2$. Then for the first half and second half following equations were used.

For the first half,

$$S_f = \left[\frac{v_f^2}{a_{\max}} \right] \text{-----} 1 \quad T = \frac{2v_f}{a_{\max}} \text{-----} 2 \quad j = \frac{a_{\max}}{\frac{T}{2}} = \frac{a_{\max}^2}{v_f} \text{-----} 3 \quad s_1(t_1) = \frac{1}{6} j t_1^3 \text{-----} 4$$

For the second half,

$$s_2(t_2) = -\frac{1}{6}j\left(t_2 - \frac{T}{2}\right)^3 + \frac{1}{2}a_{max}\left(t_2 - \frac{T}{2}\right)^2 + \frac{v_f}{2}\left(t_2 - \frac{T}{2}\right) + s_1\left(\frac{T}{2}\right) \quad \text{----- } 5$$

Then the following graph was plotted with a ramp and without ramping. The red line is for without ramping and the blue line is for the ramped profile.

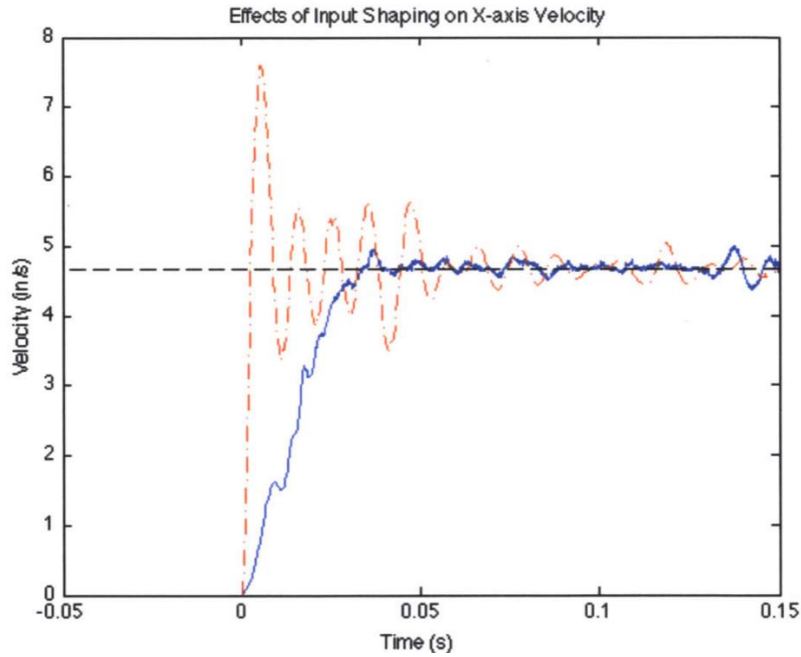


Figure 3.19: A comparison between the velocity of the X-axis without the ramping and with ramping [36].

Lan J *et al.*[36] have used a timing belt for their robots. It reduces the backlash of the belts. A DC motor was used to actuate the axis, paired with a linear encoder to register position. It reduces losing steps in stepper motors and varying the position due to the low stiffness of the belts.

3.4 Research gap

Wire Arc Additive Manufacturing (WAAM) has attracted attention in recent years because of its high rate of deposition, material utilization, and the possibility of creating large metallic structures. The majority of currently available systems either utilize high-cost robotic arms with proprietary control or high-end sensor integration, which is not suitable for small-scale or educational purposes. Though MIG welding has been found to be the most suitable process for WAAM taking cost-effectiveness and flexibility into account, a lack of inexpensive, open-

source implementations that integrate MIG welding with a gantry-based robotic platform can be seen.

Recent literature emphasizes the necessity for thermal management and optimization of process parameters in WAAM but most of these are based on expensive cooling systems, closed-loop control with expensive laser sensors, or post-processing-intensive fabrication methods which are not feasible with low-cost applications. Moreover, although simulation studies employing packages like ANSYS DED provide meaningful information regarding heat transfer and residual stress formation, little effort has been made in verifying such simulations experimentally with trials in low-cost custom-made WAAM equipment.

Another important deficiency is arc length control automation in low-cost systems. Although various sensing methods such as arc voltage feedback and laser displacement sensors have been proposed, these are expensive or extremely hard to adopt using open-source software such as Marlin or GRBL. There is little published literature on using indirect arc current feedback as a control strategy for maintaining a constant arc length in low-cost systems without commercial-grade sensors.

Lastly, while various studies focus on material testing and mechanical properties validation, they typically address high-capacity industrial WAAM systems. As a different approach, this project targets fundamental WAAM capability with off-the-shelf hardware and is thus one of the handful that looks into cost-effective, repeatable, and educational-scale WAAM development.

4 Project Workflow

Under this section we will be describing how we developed the project until we obtained experimental results.

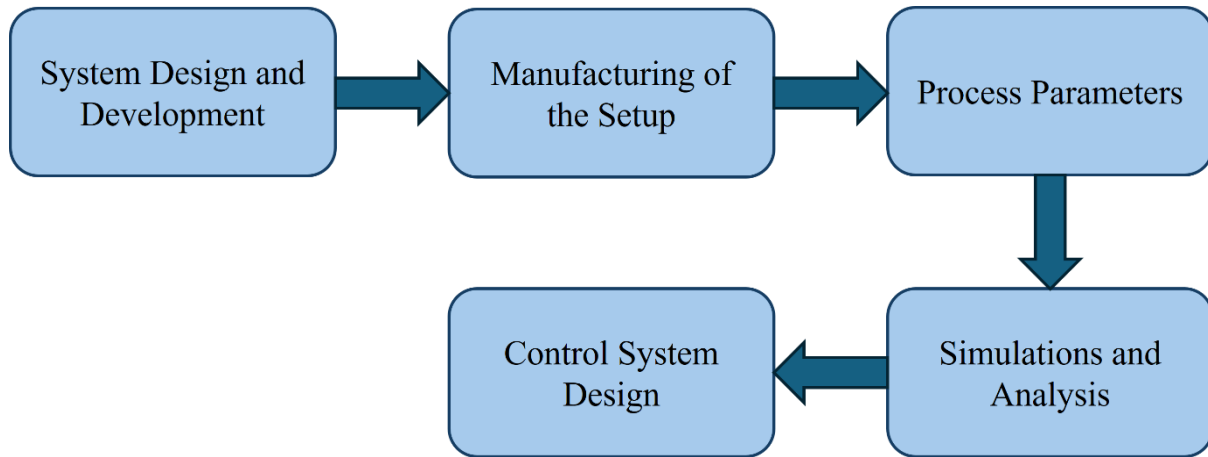


Figure 4.1: Project Workflow

4.1 System Design and Development

The design and development of the proposed metal additive manufacturing system integrated mechanical, electrical, and software components to realize a fully functional prototype capable of executing MIG-based metal deposition with motion control. The system was designed to be modular, cost-effective, and based on open-source hardware with custom designs and firmware to facilitate easy modification and future expansion.

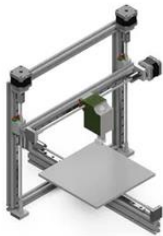
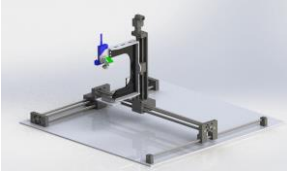

4.1.1 Conceptual Design of the Printing System

The initial phase of the project focused on the conceptual development of the system architecture. After the Literature review, the primary goal was to develop a WAAM-based metal 3D printer using MIG welding integrated into a gantry-type robotic system. The key design criteria for our project included affordability, repeatability, structural rigidity, thermal resistance, and adaptability to experimental parameter changes.

The system was designed to have three linear axes (X, Y, Z) controlled using stepper motors to control the position of the welding torch. A fixed build platform (Weld Bed) was used to simplify the design. The metal deposition process was intended to be layer-by-layer, guided by G-code generated from sliced 3D models. Safety, motion precision, and smooth integration between hardware and firmware were prioritized during the design phase.

Shown below in the Table 4-1 below is the comparative analysis performed to select the most suitable gantry design.

Table 4-1: Gantry type Comparison

	Bed Slinger	Cantilever	Stationary Bed
			
Motion type	Print bed moves along Y-axis, print head moves on X and Z axes.	Print head moves along X and Z axes, bed moves on Y-axis and is supported on one side.	Bed is fixed; gantry moves print head along X, Y, and Z axes.
Advantages	<ul style="list-style-type: none"> • Simple design • Easy to build and maintain • Inexpensive components 	<ul style="list-style-type: none"> • Compact footprint • Good visibility of print • Simple motion system 	<ul style="list-style-type: none"> • High stability • Suitable for heavy parts • Better accuracy and quality
Disadvantages	<ul style="list-style-type: none"> • Limited print speed due to bed inertia • Reduced accuracy for large parts 	<ul style="list-style-type: none"> • Susceptible to Z-axis wobble • Limited structural rigidity for tall prints 	<ul style="list-style-type: none"> • Complex assembly • Higher cost • Requires more precise calibration

For metal additive manufacturing it is required to have higher stability and better accuracy for arc generation and more flexibility. Since the weld is heated to higher temperatures a stationary weld bed is a more suitable option.

4.1.2 Gantry System Architecture

Frame and Motion Design

A rigid frame structure was constructed using Steel box bars and welded together to create a structure (Figure 4.2: Steel Structure) to hold the gantry system. A suitable height for weld bed and gantry setup was selected for the ease of operation and safety. After that 2040 aluminium profiles were used to serve as the base of the gantry system (Figure 4.3: Gantry System).

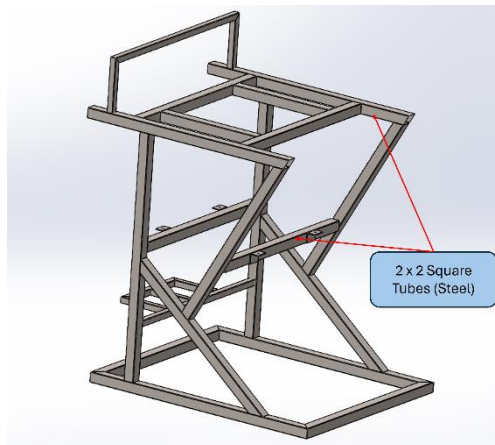


Figure 4.2: Steel Structure

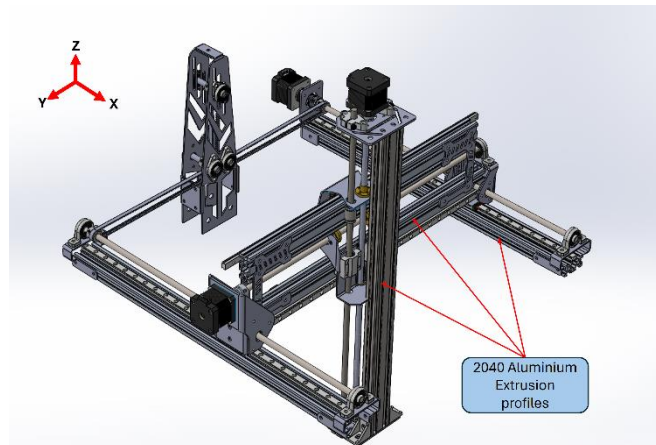


Figure 4.3: Gantry System

Linear motion along the X and Y axes was facilitated by smooth rods and linear bearings, while the Z-axis was supported using a leadscrew mechanism to allow vertical movement of the welding torch. The motion system was carefully designed to support the weight of the MIG torch and maintain stability during deposition.

Motion control was executed through belt-pulley system for the X axis to control the parallel linear guide rails and the movement of the X axis was obtained through a power screw drive system. A belt tensioning mechanism was added, so that the belt can be tensioned for our custom requirements. Y axis movement was obtained through a power screw system and linear guide rails were used to ensure high-speed movement. Two linear guide rails were used to avoid movement restrictions due the load of the welding torch. Whereas the Z-axis used a screw-drive system with two shafts for fine vertical adjustments. Each axis was driven using NEMA 17 stepper motors mounted at strategic locations on the frame. The brackets used for the motor mounting were 3mm thick sheet metal components which were capable of bearing the torque of the motors to move the gantry system.

Stepper Motors and RAMPS 1.4 Controller

The motion control system consisted of NEMA 17 stepper motors controlled using TMC2209 stepper drivers, interfaced with an Arduino Mega 2560 board. The Arduino was connected to

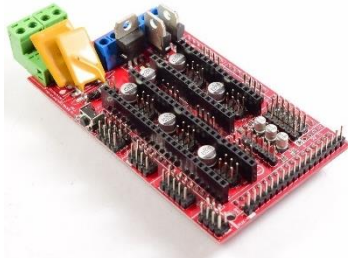


Figure 4.4: RAMPS 1.4



Figure 4.5: Arduino MEGA

a RAMPS 1.4 shield, which served as the central controller for all motion commands. The system was powered through an external 12V DC supply unit.

The RAMPS 1.4 board offered modular expansion and compatibility with open-source firmware (Marlin), making it ideal for the customizations we needed. End stops were installed on each axis to define home positions and ensure travel limits for safe operation.

4.1.3 Electrical and Firmware Setup

Arduino & Marlin Firmware Configuration

The Arduino Mega used Marlin 1.1.9.1 firmware and was configured to interpret G-code instructions and convert them into stepper motor signals. The configuration was modified to accommodate the gantry system's travel limits, motor directions, step counts, and motion speeds. Extruder and temperature control functions were disabled in the firmware, since they were not applicable for this welding-based setup.

G-code was sent via Pronterface (a host software) through USB communication to the RAMPS controller. Marlin's manual control features enabled easy axis movement and testing before printing trials. Therefore, we were able to simulate the gantry system movements before they were uploaded to the controller board. For further clarification, we used NC viewer an online tool to simulate the G code to identify possible errors.

Wiring and Safety Considerations

The system wiring included stepper motor drivers, limit switches, power supply connections, and grounding for the MIG unit. High-current wires were insulated separately to prevent arcing.

All connections were enclosed in protective casings, and the machine frame was grounded properly.

4.1.4 Welding Unit Integration

RETOP MIG-275 Setup

The welding source selected for the project was a RETOP MIG-275, an industrial-grade MIG welder donated for the development. This unit supported variable wire feed rate (WFR), voltage, and current settings, making it ideal for testing various process parameters. The welder was manually operated during early stages and later synchronized with the motion control system.



Figure 4.6: Retop MIG 275

Proper grounding and wire feed calibration were ensured before integration. The control interface of the welding unit was isolated from the microcontroller to prevent electrical noise and safety hazards.

Torch Mount and Nozzle Positioning

A customized mount was fabricated using heat-resistant materials to securely hold the welding torch. The torch was aligned perpendicularly to the build platform, and the stand-off distance (torch-to-substrate) was adjusted to control the arc length. The mount allowed minor angular adjustments and height modifications for testing different geometries and torch orientations.

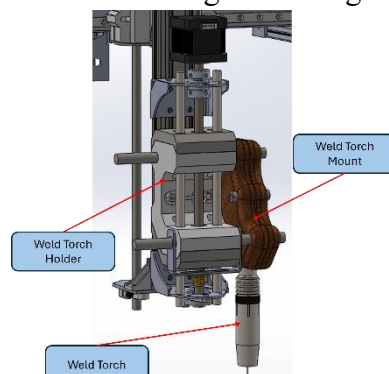


Figure 4.7: Torch Mount

4.1.5 Slicing and G-code Generation

To translate CAD models into motion instructions, **Ultimaker Cura** was used as the slicing software. Standard PLA-based printer settings were customized to suit the requirements of metal deposition. The G-code output from Cura was modified manually by removing temperature control commands and included delays and retraction instructions suitable for welding pauses for cooling.

The slicing layer height was adjusted based on the expected weld bead thickness, typically between 1.5 mm to 2.5 mm per layer. A height was obtained from manual testing. Custom post-processing scripts were developed to align welding wire feed and arc control with motion commands.

4.1.6 Workflow Automation and Control Flow

The overall system workflow consisted with the following sequence:

1. CAD modeling and STL export of the component.
2. Slicing in Cura and post-processing of G-code.
3. Uploading and sending G-code via Pronterface.
4. Coordinated movement of the gantry and torch using stepper motor control.
5. Simultaneous activation of the welding unit during torch movement.
6. Manual and software-based monitoring of bead formation.

The entire system was tested iteratively to ensure that the welding, motion, and slicing pipelines operated smoothly with minimal human intervention during execution. Also, multiple current and voltage values were obtained as data for transfer function modelling.

4.2 Manufacturing of the Setup

The manufacturing phase involved the realization of the system's conceptual and mechanical design into a prototype that can function. This covered the fabrication of the frame, installation of mechanical and electrical subsystems, and final integration of the welding and motion control components. Careful attention was given to ensure structural rigidity, electrical safety, and reliable motion performance throughout the build process

4.2.1 Fabrication of Structural Components

The rigid frame was fabricated after cutting and welding the 2-inch x 2-inch box bars according to the dimensions of the CAD file. Then gantry frame was constructed primarily using aluminium extrusion profiles, chosen for their balance between strength, weight, and modularity. The fabrication process involved precise cutting of aluminium profiles to desired lengths using a chop saw, followed by drilling and tapping to enable the mounting of joining brackets and components. (Refer Figure 8.7: Steel Box Bar Structure)

The frame was assembled on a levelled platform to ensure orthogonality and squareness across all axes. Brackets and T-slot fasteners were used to rigidly fix the vertical and horizontal members. Brackets were fabricated by laser cutting and bending sheet metal with the required thicknesses. Additional reinforcements such as L-brackets were added at high-load regions to minimize flexing during torch movement.

4.2.2 Installation of Motors, Rails, and Lead Screws

Once the frame was complete, linear rails and motion systems were installed. The X and Y axes used linear rail guides for low-friction motion with lead screws and brass T nuts. while the Z-axis incorporated a lead screw and brass nut with two smooth rods with linear bearings to ensure accurate vertical displacement. All the mounting sheet metal brackets were laser cut and bended for manufacturing.

NEMA 17 stepper motors were mounted onto the frame using custom-designed brackets which were also later cut and bended. GT2 pulleys and timing belts were attached to the motors on the X axes, and the belt tensioning unit was also fabricated using sheet metal but laser cutting and bending. Alignment and tensioning were critical in minimizing backlash and ensuring smooth operation during printing.

T-nuts and Allen bolts were used to attach the brackets to the extrusion profiles and brackets to the bearings.



Figure 4.9: Manufactured brackets



Figure 4.8: Pulley tensioning unit

4.2.3 Torch Holder and Z-Axis Assembly

A custom torch holder was fabricated using a heat-resistant aluminium bracket designed to securely clamp the MIG torch in position. The mount was connected to the Z-axis carriage and designed to allow vertical adjustment to control arc length.

The torch holder also included minor angular flexibility for testing different torch orientations during experimental trials. Adequate clearance was provided to accommodate the wire feed and shielding gas flow from the RETOP MIG-275 unit.



Figure 4.10: Z-Axis Assembly

4.2.4 Cable Management and Safety Features

As the motion system and welding unit introduced multiple wiring paths, effective cable management was essential. Stepper motor wires, and power cables were bundled using flexible cable sleeves and routed through drag chains to avoid entanglement with moving parts.

High-current MIG power cables and signal wires were kept isolated from each other to reduce electrical noise. The entire frame was properly grounded, and safety features such as emergency stop buttons and current limiters were incorporated. A clear acrylic shield was used to enclose the deposition area for operator safety during welding.

4.2.5 Integration and Full System Assembly

After individual subsystems were installed, the entire setup was integrated and tested. The welding torch was connected to the power source, and the stepper motors were interfaced with the RAMPS 1.4 control board. The firmware (Marlin) was configured and uploaded to the Arduino Mega to enable communication with the host software (Pronterface).

A series of calibration steps were performed:

- Z - axis end-stop which was a load cell was configured.
- Verifying movement range and alignment.
- Performing dry runs of G-code motion without activating the welder.
- Testing the torch activation timing and wire feed control.

The full system underwent multiple verification rounds before experimental printing trials commenced. This marked the successful transition from design to a fully functional metal additive manufacturing prototype.



Figure 4.11: Prototype

4.3 Process Parameters

The quality and consistency of the deposited weld bead in WAAM systems depends highly on the selection and tuning of process parameters. These includes voltage, current, wire feed rate (WFR), and travel speed. The study of these parameters was carried out through manual trials, empirical observations, and iterative tuning. The aim was to determine the most suitable combination of values that generate a stable arc, uniform bead geometry, minimal spatter and constant power while maintaining efficient metal deposition.

4.3.1 Key Parameters: Voltage, Current, WFR, Travel Speed

We were able to identify several key process parameters as critical to the WAAM process using MIG welding:

- Voltage (V): Controls the arc length and affects the fluidity of the weld pool. Higher voltage tends to increase the arc length and flatten the bead profile.
- Current (A): Directly influences the heat input and penetration depth. It is largely dependent on the wire feed rate and is adjusted through the welding machine along with the WFR.
- Wire Feed Rate (WFR): This determines the rate of filler material is supplied to the weld pool. It is one of the most important parameters affecting bead height and continuity.
- Travel Speed (TS): The speed, which the welding torch moves relative to the substrate. It affects bead width, penetration, and heat input distribution.

A balance between these parameters is required to ensure consistent metal deposition without defects such as porosity, undercut, excessive spatter, or irregular bead shapes

4.3.2 Preliminary Manual Testing Results

Initial experiments were conducted using manual control of the welding process while the gantry system was operated via G-code-based motion. During these trials, various combinations of current, voltage, and WFR were tested to observe the behaviour of the arc, the wetting of the substrate, and the resulting bead shape.

Some key observations during preliminary tests included:

- High voltage and low wire feed resulted in excessive arc length, leading to bead irregularities and poor fusion.
- Low voltage with high wire feed caused arc instability and inconsistent deposition.
- Excessive travel speed led to thin, under-filled beads, while very slow speeds caused excessive heat input, leading to warping or large bead widths.

These observations guided the selection of a narrower parameter range for further optimization.

4.3.3 Effects of Parameters on Bead Geometry

A systematic study was carried out to examine how individual parameters influenced bead characteristics such as width, height, penetration depth, and surface uniformity. Test lines were printed at constant values while varying one parameter at a time.

Key findings:

- Increasing voltage resulted in wider and flatter beads but reduced penetration.
- Higher current/WFR improved build height but could lead to excessive reinforcement and spatter if not matched with adequate travel speed.
- Faster travel speed produced narrower beads with reduced height and poor fusion.
- Optimal combinations of high WFR with moderate voltage and low-to-medium travel speed produced uniform, stable beads.

Photographic and dimensional analysis of the beads was used to evaluate the quality of deposition and identify the acceptable process window.

4.3.4 Empirical Calibration and Iterative Testing

Based on preliminary results, a series of iterative tests were performed where parameter values were incrementally adjusted, and the resulting bead geometries were measured and recorded. The calibration process involved:

- Printing straight-line segments with varying parameters.
- Measuring bead width and height using callipers.
- Recording visual defects such as spatter, lack of fusion, or inconsistent flow.
- Comparing the results against simulation predictions from ANSYS DED.

Each round of testing informed the next set of parameter values, gradually converging toward a reliable set of operating conditions. This empirical approach allowed us to refine both the motion control speed and the welding input to maximize consistency and quality.

4.3.5 Operating Envelope Identification

Through extensive manual testing and calibration, a practical operating envelope was established—a range of parameter values within which the system could reliably operate without introducing defects.

The optimal range for key parameters was identified as:

- Voltage: 20–25 V
- Current: 120–140 A
- Wire Feed Rate: 6–8 m/min
- Travel Speed: 1000 mm/min

Within this envelope, the arc remained stable, and the deposition process produced smooth, well-bonded layers with minimal distortion. These parameters were adopted for subsequent experimental trials and simulation validation. Any deviation outside this range led to significant quality degradation or process instability.

This identified envelope serves as the foundation for automated deposition paths and enables reliable layer-by-layer metal printing using the developed MIG-based WAAM system.

4.4 Simulation and Analysis

To enhance process understanding and to support parameter identification, simulations were performed using ANSYS Additive Wizard (Directed Energy Deposition module). The simulations aimed to replicate the WAAM process virtually and predict key physical phenomena such as heat distribution, thermal cycling, residual stresses, and deformation. This simulation-based approach provided valuable insights that guided the selection of process parameters and helped anticipate potential defects during the actual fabrication process.

4.4.1 Simulation Objectives and Strategy

The primary objectives of the simulation were:

- To predict temperature distribution within the printed layers and the substrate.

- To evaluate thermal gradients and their influence on residual stress formation.
- To assess layer deformation and potential warping during the build process.
- To validate the physical printing results against thermal and structural behaviour predicted by the simulation.

The simulation strategy involved importing the sliced G-code of simple geometries (e.g., straight wall and cylindrical samples), defining the material properties, boundary conditions, and energy input, and then evaluating thermal-mechanical coupling across the printed layers.

4.4.2 Geometry and Model Preparation

Multiple geometries were selected for simulation:

- Model 1: A two-layer straight wall (linear path deposition)
- Model 2: A two-layer cylindrical geometry (curved path deposition)
- Model 1: A five-layer straight wall (linear path deposition)
- Model 2: A five-layer cylindrical geometry (curved path deposition)

The 3D models were created using SolidWorks, exported as STL files, and sliced using Ultimaker Cura. The G-code was manually customized to be compatible with the simulation inputs in ANSYS. Mesh refinement was conducted using Cartesian meshing, with finer mesh sizes around the deposition path and coarser mesh away from the heat-affected zone (HAZ)(Weld Bed) to reduce computational cost.

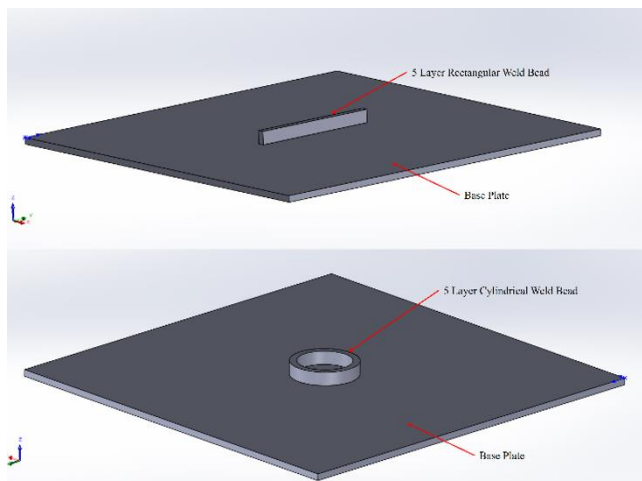


Figure 4.12: Geometry Models

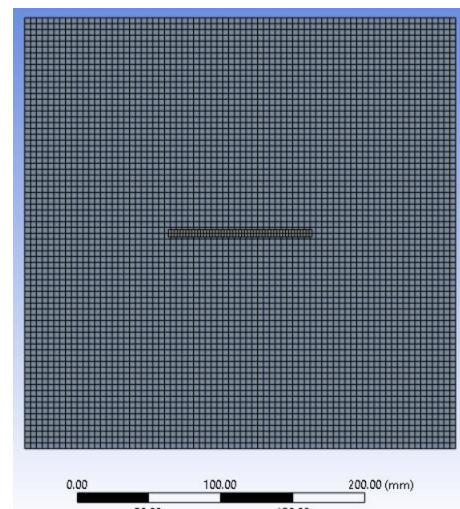


Figure 4.13: Cartesian mesh

4.4.3 G-code Integration and Toolpath Definition

The customized G-code was interpreted within the ANSYS Additive Wizard to define the deposition path. Each layer's toolpath was specified based on the time step, with deposition segments assigned appropriate material activation and energy input commands. The movement of the heat source (representing the MIG arc) was synchronized with the predefined deposition path.

The simulation assumed a constant deposition rate and uniform layer thickness, which were aligned with the average bead dimensions observed in experimental trials.

4.4.4 Thermal Analysis using ANSYS DED

The thermal analysis was conducted to understand how heat propagates through the deposited material and the substrate. The following were set as inputs:

- Material: Mild Steel (ER70S-6 wire equivalent)
- Heat Source: Gaussian volumetric heat input model
- Input Power: Calculated using $P=V \times I$ (based on empirical values)
- Initial Conditions: Ambient temperature at 25°C
- Boundary Conditions: Natural convection applied to free surfaces

Results showed that:

- Peak temperatures at the melt pool reached above 1290°C.
- Heat was conducted into the base plate with significant gradients between layers.
- Thermal accumulation occurred in higher layers, influencing layer bonding and potential warping

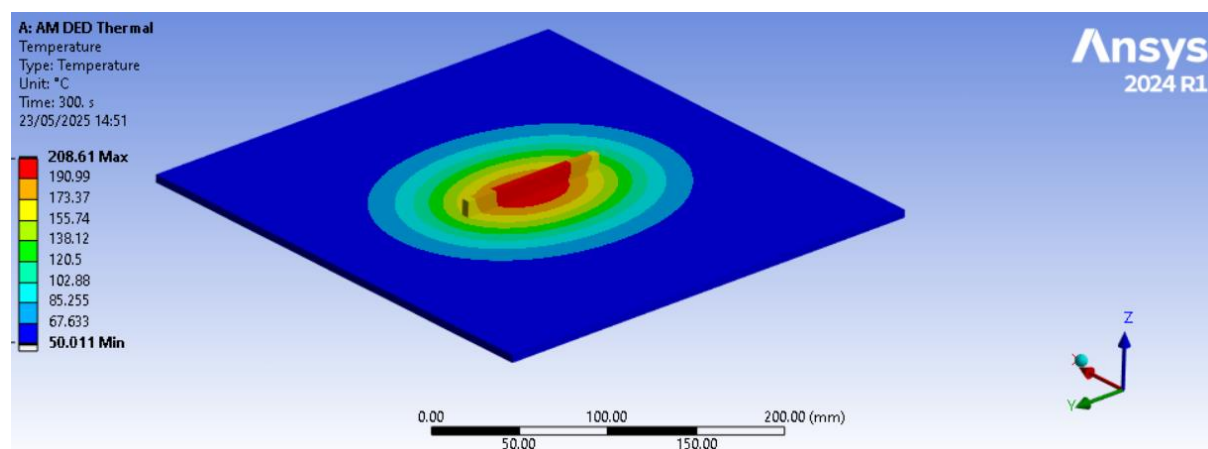


Figure 4.14: Thermal Simulation result After 300s Cool down for rectangular weld Bead

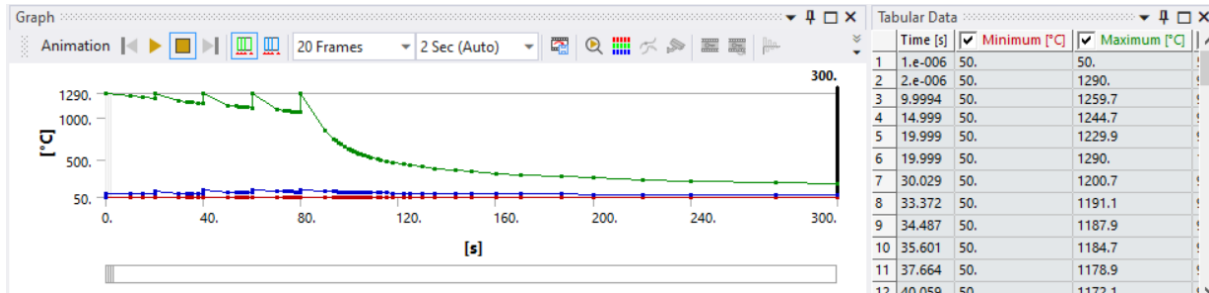


Figure 4.16: Thermal Simulation Graph during Layer-by-layer metal deposition

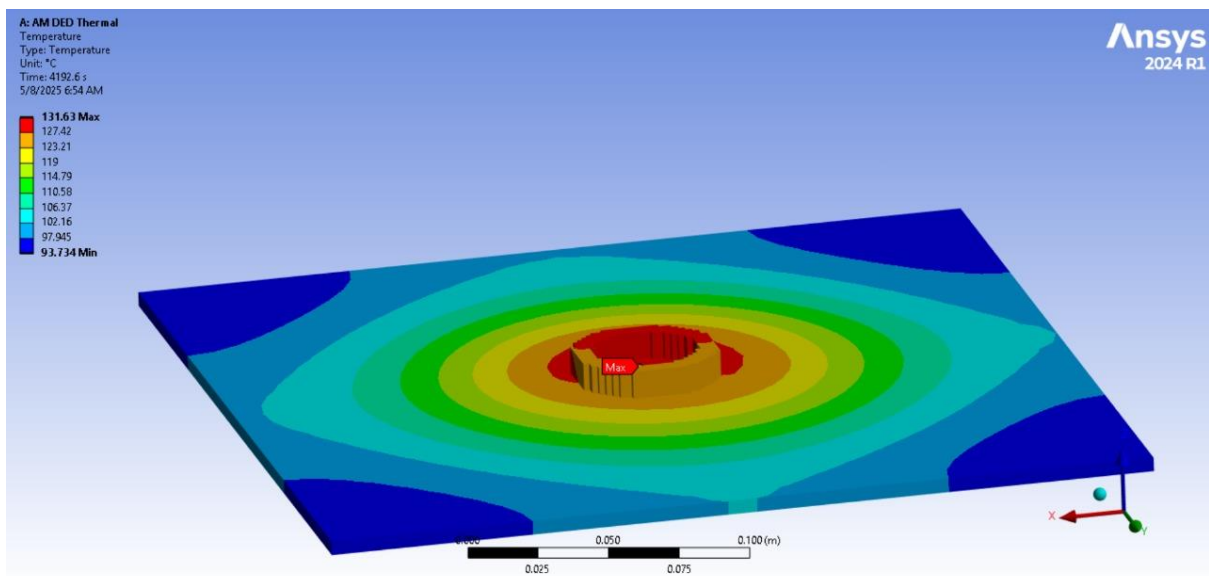


Figure 4.15: Thermal Simulation Results After 4000s Cooldown for Circular Weld Bead

4.4.5 Residual Stress and Deformation Prediction

Following the thermal simulation, a coupled thermal-structural analysis was performed to calculate residual stresses and deformations resulting from thermal expansion and contraction during solidification.

Findings from the simulation:

- Residual tensile stresses were highest near the top deposited layers.
- Compressive stresses were observed at the base due to constraint from the substrate.
- Slight upward warping was predicted in the edges of the wall model.

- The cylindrical model exhibited radial shrinkage, which was confirmed in physical tests.

These stress distributions align with the typical patterns observed in WAAM processes and highlight the importance of optimized cooling and clamping strategy.

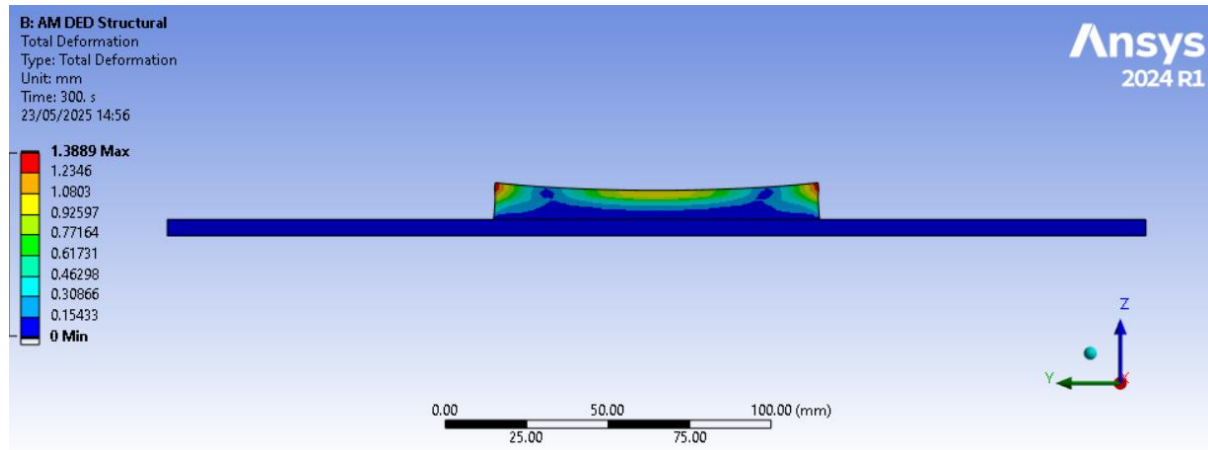


Figure 4.17: Deformation Results for rectangular weld Bead

4.4.6 Result Interpretation and Process Refinement

The simulation results were compared with experimental findings such as bead size, deformation, and overall print quality. The consistency between predicted and actual temperature zones, stress locations, and warping tendencies validated the simulation setup.

Based on the results:

- Preheating of the base plate was identified as a potential method to reduce thermal gradients.
- Travel speed and layer cooling time were fine-tuned to minimize distortion.
- The validated simulation model can be used for future studies to predict complex geometries and optimize process planning.

4.5 Control System Design

The control system for the developed metal additive manufacturing system was designed with three main objectives:

1. Controlling the gantry motion system,

2. Automating the activation of the MIG welding torch, and
3. Monitoring arc-related parameters, including current, to support future control of arc length.

These control functions were implemented by a combination of open-source firmware, embedded electronics, analog signal processing, and custom scripting. A significant emphasis was placed on maintaining low-cost and modular design principles while ensuring real-time responsiveness and operational safety.

4.5.1 Gantry Motion Control

The primary motion control along X, Y, and Z was implemented using an Arduino Mega 2560 interfaced with a RAMPS 1.4 board. Three NEMA 17 stepper motors—each controlled via TMC2209 drivers—were assigned to the X, Y, and Z axes of the gantry system. The Marlin 1.1.9.1 firmware was uploaded onto the Arduino to handle G-code instructions, allowing precise control over travel speed, path, and deposition order.

Pronterface software was used as the G-code hosting interface, enabling manual control and automated printing for ease of calibration. Travel limits, axis directions, and acceleration values were configured in the firmware to suit the system's mechanical design while Axis calibration, feed-rate adjustments, and G-code monitoring were all performed through the Pronterface.

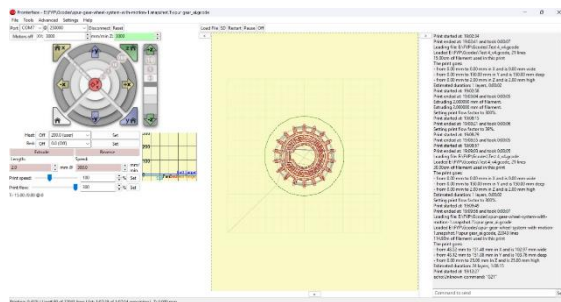


Figure 4.19: Pronterface user Interface

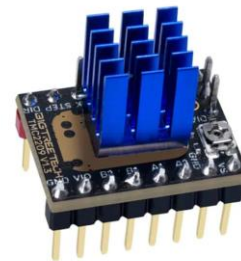


Figure 4.18: TMC 2209

4.5.2 Starting Point Detection with Load Cell

To determine the starting point for metal deposition, the default bed-leveling feature in Marlin firmware was modified for this application. A load cell module connected via an HX711 amplifier was integrated to detect the moment when the torch tip made contact with the base plate (welding bed).

The HX711 module was triggered with the auxiliary pins on the RAMPS 1.4 board, and custom firmware modifications were done to read the load readings. When the measured force exceeded a defined value, the Z-axis stepper motor was programmed to retract the torch by 2 mm, establishing the arc initiation point.

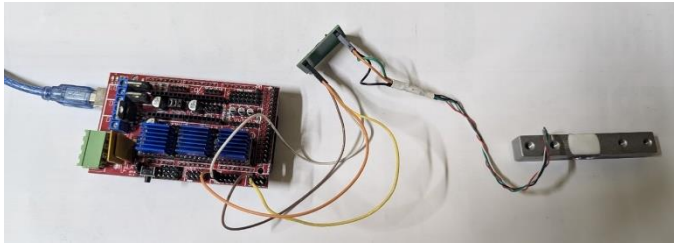


Figure 4.20: Calibration Setup

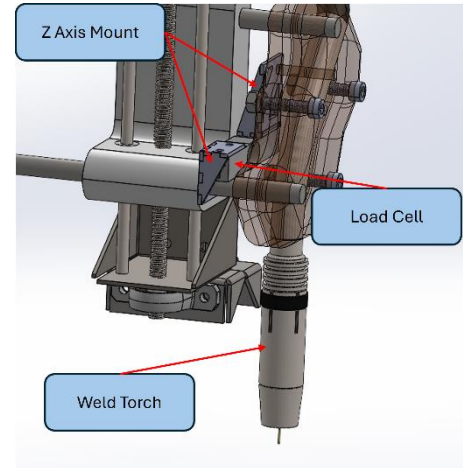


Figure 4.21: Load Cell Mounting

4.5.3 Welding Torch Activation Using Extruder Signal

In order to synchronize the activation of welding torches with the running of G-code, the system used the extruder step signal on the RAMPS board and rotated a stepper motor. The Stepper motor was connected to a rotary encoder as shown in the figure below. The signal from the encoder was conditioned to feed a 5V mechanical relay that turned on the welding torch switch. since the encoder gives rotational signals were used as high while non rotation moments were used as low signals to switch on and off the welding torch.

The altered extruder pulse was therefore capable of actuating the relay reliably in print jobs to initiate arcs and synchronize deposition.

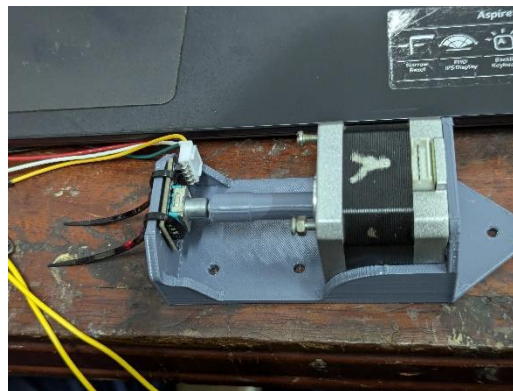


Figure 4.24: Setup to Read the extruder signal

4.5.4 Real-Time Welding Current Measurement

Understanding the dynamic behavior of the arc during deposition is crucial for defect minimization. The RETOP MIG-275 welding machine includes analog-style displays for real-time voltage and current, which were leveraged for process monitoring.

An oscilloscope was used to identify the signal path driving the current display. This signal was determined to be an analog voltage proportional to the welding current. A calibration process was performed using a DC power supply, where known voltages were input to map their corresponding display readings.

This analog signal can be further processed in future iterations using an ADC (Analog-to-Digital Converter) to support closed-loop feedback systems for arc length or current control.

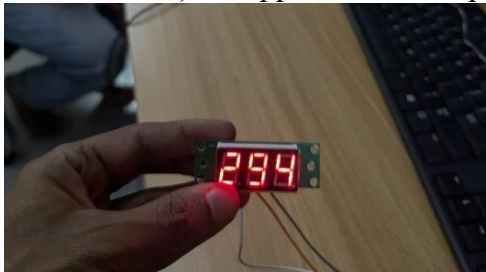


Figure 4.26: The current display unit

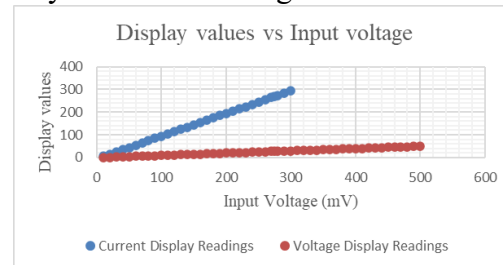


Figure 4.25: Calibrated Values

4.5.5 Constant Arc Length Control

Maintaining a consistent arc length is essential to ensure uniform bead geometry and thermal stability. In this system, arc length control was indirectly achieved by monitoring the arc current and adjusting the Z-axis height accordingly. As per literature and experimental results:

- Arc current decreases with increasing arc length due to rising electrical impedance.
- Arc current increases as the torch gets closer to the workpiece.

To compensate, a secondary stepper motor was connected in parallel with the Z-axis to enable fine vertical adjustments during printing. The control logic was:

- If current < target, the Z-axis moves downward to reduce arc length.
- If current > target, the Z-axis retracts slightly.

Theoretical Modeling

To find the best voltage and the current for welding, the welding power was considered. The change in arc power with the voltage was given by,

$$\frac{d(VI)}{dV} = I + V \frac{dI}{dV}$$

The power source characteristic to be a straight line given by the equation,

$$V = V_0 + mI$$

$$\frac{d(VI)}{dV} = I + \frac{1}{m} V$$

At maximum power,

$$I + \frac{1}{m} V = 0 \Rightarrow \frac{V}{I} = -m$$

For the MIG welding machines,

$$m = -0.125$$

This method was used in MATLAB to find the optimum voltage and the current values for a given welding power value.

Arc Length Estimation Model

Using physical properties and literature data, a MATLAB-based equation was used to relate arc length to arc current:

$$l_A(U_T, I) = \frac{U_T - U_{F0} - (R_F + R_{W0} + \rho_W l_{CTWD})I}{E_{z0} + (\rho_z - \rho_W)I}.$$

l_A	Arc length (mm)
U_T	Total arc voltage (measured between contact tip and workpiece)
U_{F0}	Fixed voltage drops in the arc plasma (near the cathode region)
R_F	Fixed resistance of cables and connectors
R_{W0}	Fixed resistance of the welding wire (excluding CTWD)
ρ_W	Resistivity of the welding wire material ($\Omega \cdot m$)
l_{CTWD}	Contact Tip to Work Distance (physical wire extension)
E_{z0}	Arc electric field strength in the arc column (V/m)
ρ_z	Specific resistivity of arc plasma column
I	Welding current (A)

This yielded a lookup table of arc length vs. arc current, visualized in Figure 4.27: Arc Length vs Welding Current, which was used to guide Z-axis correction behavior during printing.

Though a fully dynamic feedback system was not completed due to time constraints, the design and logic provide a foundation for future implementation of a closed-loop arc length control system using current sensing and PID control.

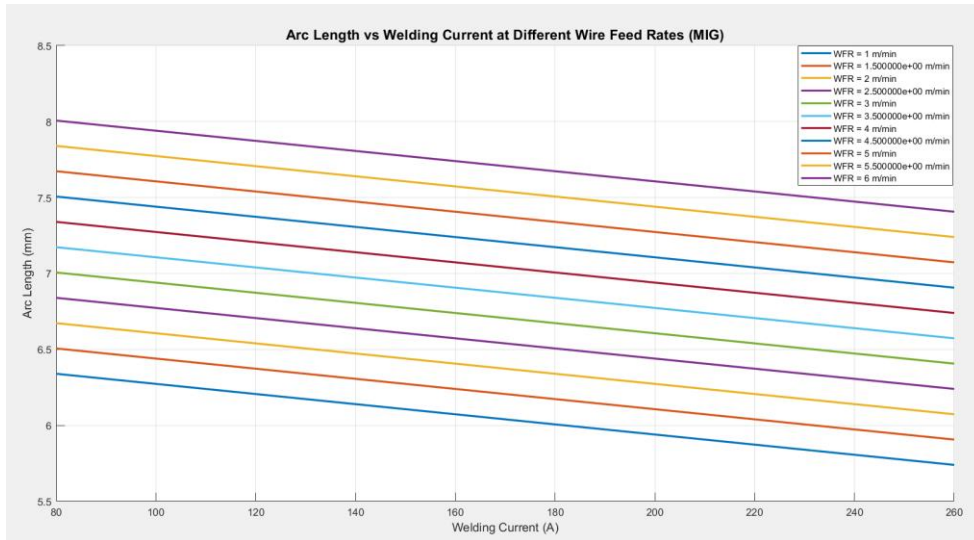


Figure 4.27: Arc Length vs Welding Current

4.5.6 Control system Block Diagram for the Arc length correction system

The control system block diagram using MATLAB SIMULINK was used to tune the PID controller of the system and get accurate results from the control system for the arc length correction system.

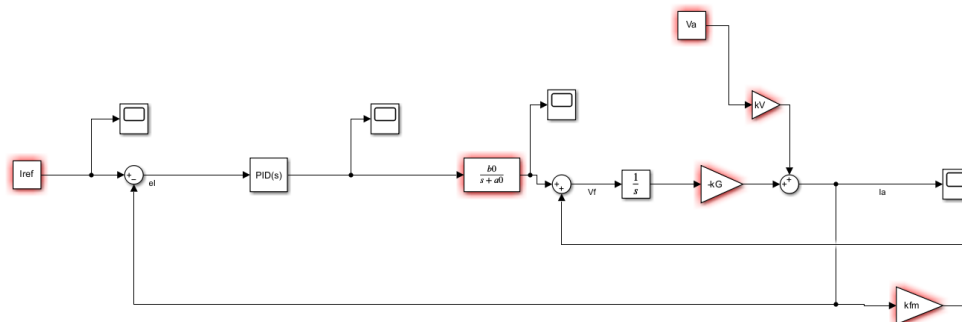


Figure 4.28: Control system block diagram in SIMULINK

I_{ref} = Reference current of the welding

V_a = welding voltage

e_i = Current error

V_f = Velocity of the stepper motor

k_{fM} = Gain of the wire feed rate controller

I_a = Welding current

k_v = Voltage gain

4.5.7 Estimate a Linear Model for the Arc length correction system Using System Identification App

The arc length was changed by the system rotating the arc length correction stepper motor and the arc current values and the rotating angle values were recorded with respect to time domain. This single input single output data was used to estimate a linear model describing the system dynamics.

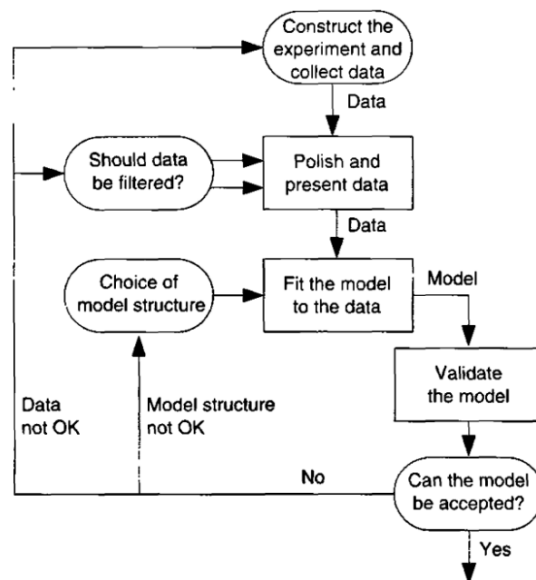


Figure 4.29: Identification cycle

5 EXPERIMENTAL TEST RESULTS AND DISCUSSION

5.1 Experimental Fabrication and Validation

This chapter describes the experimental validation of the metal additive manufacturing system designed. Printing feasibility, dimensional tolerance, and weld bead formation were evaluated through a series of tests. The results are compared with predictions from the simulation model to establish accuracy and reliability. The discussion further analyses the effects of various parameters, problems faced, and lessons learned while conducting the trials.

5.1.1 Material Selection and Test Samples

The experimental trial welding wire chosen was ER70S-6 mild steel (diameter: 0.8 mm) because of its extensive availability, good weldability, and GMAW suitability. The substrate used was a 3 mm thick mild steel plate. These were chosen to save costs and to ensure compatibility with the RETOP MIG-275 welder. Test specimens involved:

- Single-bead straight lines (50 mm in length)
- Multi-layer rectangular buildings (up to 5 layers)
- Circular path samples for initial geometric complexity checking

5.1.2 Printing Trials and Bead Formation

The initial experiments included the fabrication of single-layer beads through manual manipulation of voltage, travel speed, and wire feed rate (WFR). The parameters utilized were derived from the optimized envelope established in previous phases:

Voltage: 22 - 25 V

Currently: 120–140 A

Wire Feed Rate: 6.5–8 m/min

Travel Speed: 1000 mm/min

Beads were deposited with success using the gantry motion system synchronized with torch activation. The deposition was stable for travel lengths of up to 100 mm.



Figure 5.2: Prototype during the Welding

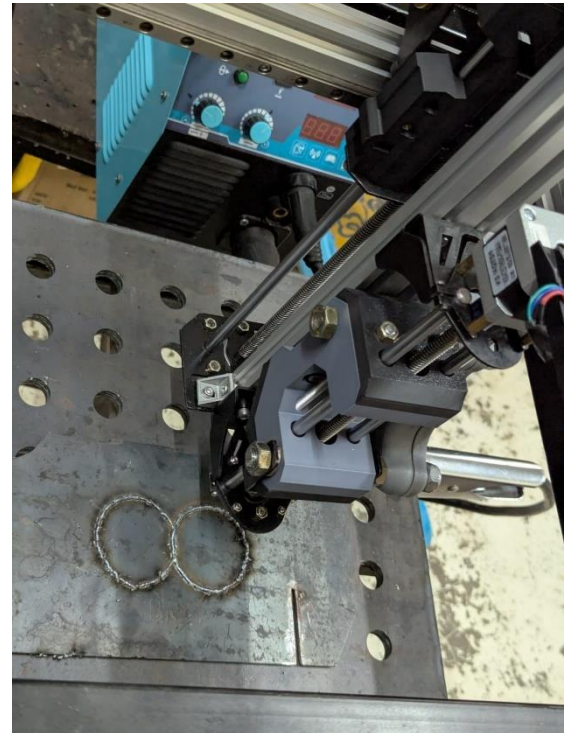


Figure 5.1: Circular Weld Bead

5.1.3 Visual and Dimensional Inspection

After the printing, all the samples were visually and dimensionally inspected:

Diameters of beads ranged from 2.5 mm to 5 mm



Figure 5.3: Wire Bead Thicknesses

Height consistency varied marginally with number of layers, with the overall trend of falling height with rising number of layers due to heat accumulation

Minimum spatter was observed when current was between 125 - 135 A

Cases of undercut and wavy edges were seen at high travel rates or reduced wire feed rates.



Figure 5.4: High Travel Speed Weld Run

Bead geometry was measured by utilizing a digital calliper, and measurements were made to improve the process.

5.1.4 Cross-Sectional Analysis

Though beyond the project scope was advanced metallurgical testing, simple cross-sectional examination was done by sectioning the deposited sample:



Figure 5.5: Cross Section of the Weld (6 weld Beads)

A cross-section macro photo taken from a mobile phone showed good integration between the layers.

No visible inclusions or significant porosity were seen in the low-speed samples.

Beads deposited with high wire feed had convex profiles and higher reinforcement

5.1.5 Comparison with Simulated Results

Simulation results from the ANSYS DED module were compared to experimental data:

The thermal field predictions closely matched the heat-affected zones observed on the substrate

Predicted residual stress regions in accordance with experimentally measured warping for longer beads

Curved print shrinkage and deformation matched simulation output, validating toolpath modelling.

The analyses proved to validate that the simulation model was a reliable prediction of WAAM performance, specifically heat distribution and distortion.

5.1.6 Lessons Learned and Process Tuning

Significant results achieved by testing include:

The significance of holding the arc length constant for the stability of beads underscores the position of current feedback.

Interpass cooling time greatly influences bead width and height.

Surface roughness can be reduced through preheating the base plate or optimizing wire stick-out.

MIG deposition G-code manual post-processing remains challenging but a necessary evil for stability.

These lessons will act as a roadmap for subsequent enhancements in toolpath design, automation of processes, and minimization of defects.

5.2 Discussion

5.2.1 Evaluation of System Performance

The WAAM system developed effectively:

- Printed simple geometries in mild steel
- Repeatedly executed steady motion and bead tracking
- The welding torch was ignited with precise timing.
- Demonstrated feedback-controlled Z-axis motion for arc length stabilisation

- While restricted in build volume and accuracy, the system was found to be workable and dependable for research-level uses.

5.2.2 Parameter Influence and Process Stability

Empirical evidence indicated:

Voltage and wire feed speed have important influences on bead shape and spatter

Travel speed impacts fusion quality and consistency

A narrow operating window (Voltage: 18–20 V; WFR: 6–8 m/min) gave best results

Deviation from these parameters led to aberrant bead formation, confirming their essential function.

5.2.3 Comparison of Experimental vs Simulated Data

Simulation results from ANSYS predicted:

- Thermal zones
- Residual stress regions
- Deformation tendencies

These agreed with experimental results in trend and magnitude, particularly in multi-layer straight-line samples, confirming the usefulness of simulation in build planning and parameter tuning.

5.2.4 Practical Challenges and Solutions

Challenges encountered:

Relay not activating each time due to the short pulse duration.

Arc instability at high-speed movements.

Manual G-code editing for welding-related commands.

Encoder used for data collection of the extruder actuation gets jammed occasionally resulting in print failures.

Implemented solutions:

Reducing travel speed and optimizing start-stop cycles.

Layer-by-layer Z-axis movement dependent on current-based control logic

5.2.5 Contributions and Implications for WAAM Development

This project contributes to WAAM research in that: Demonstrating a low-cost MIG-based metal 3D printer prototype Explaining the utilization of arc current feedback in controlling arc length Introducing a simulation-based process optimization system Offering a modular control design to permit future closed-loop upgrades The findings are encouraging for further investigation of low-cost, open-source WAAM hardware for SME use and educational applications in developing countries like Sri Lanka.

5.2.6 Future work

Although a basic control system was successfully implemented and tested, the foundation has been laid for further enhancements, including:

- Closed-loop arc length control using real-time current feedback and Z-axis compensation.
- Temperature-based control with cooling fan integration or thermal shutdown logic.
- Adaptive G-code control, where deposition speed or arc characteristics are adjusted dynamically based on sensor feedback.

These advancements would enable more precise deposition, reduce common WAAM defects, and transition the system closer to industrial-grade control capabilities.

6 CONCLUSIONS

In conclusion, the project was able to prove a concept of designing and developing a low-cost metal additive manufacturing system based on MIG welding and a three-axis gantry robust robotic platform. The system was capable of making simple metal components with acceptable degree of dimension accuracy and structural soundness, as validated through design, simulation and experimental verification. The simulation tools also integrated with the process and gave important information regarding the optimization of the process parameters, using which the control system was developed which will provide future automation should it be required. This work does offer a good basis of pushing into developing more accessible metal additive manufacturing technologies despite the limitations that it offers, as there are a few such as closed-loop control and the production of complex geometries in the manufacturing process.

7 REFERENCE

- [1] S. W. Williams, F. Martina, A. C. Addison, J. Ding, G. Pardal, and P. Colegrove, “Wire + Arc additive manufacturing,” *Materials Science and Technology (United Kingdom)*, vol. 32, no. 7, pp. 641–647, Jun. 2016, doi: 10.1179/1743284715Y.0000000073.
- [2] F. Martina, J. Mehnen, S. W. Williams, P. Colegrove, and F. Wang, “Investigation of the benefits of plasma deposition for the additive layer manufacture of Ti-6Al-4V,” *J Mater Process Technol*, vol. 212, no. 6, pp. 1377–1386, Jun. 2012, doi: 10.1016/j.jmatprotec.2012.02.002.
- [3] F. Wang, S. Williams, P. Colegrove, and A. A. Antonysamy, “Microstructure and mechanical properties of wire and arc additive manufactured Ti-6Al-4V,” *Metall Mater Trans A Phys Metall Mater Sci*, vol. 44, no. 2, pp. 968–977, Feb. 2013, doi: 10.1007/s11661-012-1444-6.
- [4] J. Ding *et al.*, “Thermo-mechanical analysis of Wire and Arc Additive Layer Manufacturing process on large multi-layer parts,” *Comput Mater Sci*, vol. 50, no. 12, pp. 3315–3322, Dec. 2011, doi: 10.1016/j.commatsci.2011.06.023.
- [5] A. Paolini, S. Kollmannsberger, and E. Rank, “Additive manufacturing in construction: A review on processes, applications, and digital planning methods,” Dec. 01, 2019, Elsevier B.V. doi: 10.1016/j.addma.2019.100894.
- [6] E. Karayel and Y. Bozkurt, “Additive manufacturing method and different welding applications,” 2020, Elsevier Editora Ltda. doi: 10.1016/j.jmrt.2020.08.039.
- [7] W. E. Frazier, “Metal additive manufacturing: A review,” 2014, Springer New York LLC. doi: 10.1007/s11665-014-0958-z.
- [8] R. Singh *et al.*, “Powder bed fusion process in additive manufacturing: An overview,” in *Materials Today: Proceedings*, Elsevier Ltd, 2019, pp. 3058–3070. doi: 10.1016/j.matpr.2020.02.635.
- [9] M. Ziaee and N. B. Crane, “Binder jetting: A review of process, materials, and methods,” Aug. 01, 2019, Elsevier B.V. doi: 10.1016/j.addma.2019.05.031.

- [10] A. Elkaseer, K. J. Chen, J. C. Janhsen, O. Refle, V. Hagenmeyer, and S. G. Scholz, “Material jetting for advanced applications: A state-of-the-art review, gaps and future directions,” Dec. 01, 2022, Elsevier B.V. doi: 10.1016/j.addma.2022.103270.
- [11] E. Aldalur, F. Veiga, A. Suárez, J. Bilbao, and A. Lamikiz, “High deposition wire arc additive manufacturing of mild steel: Strategies and heat input effect on microstructure and mechanical properties,” *J Manuf Process*, vol. 58, pp. 615–626, Oct. 2020, doi: 10.1016/j.jmapro.2020.08.060.
- [12] N. A. Rosli *et al.*, “Design and development of a low-cost 3d metal printer,” *Journal of Mechanical Engineering Research and Developments*, vol. 41, no. 3, pp. 47–54, 2018, doi: 10.26480/jmerd.03.2018.47.54.
- [13] A. Puzatova, P. Shakor, V. Laghi, and M. Dmitrieva, “Large-Scale 3D Printing for Construction Application by Means of Robotic Arm and Gantry 3D Printer: A Review,” Nov. 01, 2022, MDPI. doi: 10.3390/buildings12112023.
- [14] C. Selcuk Dr, “Joining processes for powder metallurgy parts,” in *Advances in Powder Metallurgy: Properties, Processing and Applications*, Elsevier Inc., 2013, pp. 380–398. doi: 10.1533/9780857098900.3.380.
- [15] D. Ding, Z. Pan, D. Cuiuri, and H. Li, “Wire-feed additive manufacturing of metal components: technologies, developments and future interests,” Oct. 26, 2015, Springer London. doi: 10.1007/s00170-015-7077-3.
- [16] Y. Nilsiam, P. G. Sanders, and J. M. Pearce, “Applications of open source gmaw-based metal 3-d printing,” *Journal of Manufacturing and Materials Processing*, vol. 2, no. 1, 2018, doi: 10.3390/jmmp2010018.
- [17] G. C. Anzalone, C. Zhang, B. Wijnen, P. G. Sanders, J. Pearce, and J. M. Pearce, “A Low-Cost Open-Source Metal 3-D Printer,” *IEEE Access*, no. 1, 2013, doi: 10.1109/ACCESS.2013.2293018.
- [18] Hidekai Nagamatsu and Hiroyuki Sasahara, “Development of a cooperative system for wire and arc additive,” *Additive Manufacturing* 31, 2020.

- [19] Y. Li, C. Su, and J. Zhu, “Comprehensive review of wire arc additive manufacturing: Hardware system, physical process, monitoring, property characterization, application and future prospects,” Mar. 01, 2022, Elsevier B.V. doi: 10.1016/j.rineng.2021.100330.
- [20] C. Xia et al., “A review on wire arc additive manufacturing: Monitoring, control and a framework of automated system,” Oct. 01, 2020, Elsevier B.V. doi: 10.1016/j.jmsy.2020.08.008.
- [21] B. Wu et al., “A review of the wire arc additive manufacturing of metals: properties, defects and quality improvement,” Oct. 01, 2018, Elsevier Ltd. doi: 10.1016/j.jmapro.2018.08.001.
- [22] T. Artaza et al., “Design and integration of WAAM technology and in situ monitoring system in a gantry machine,” in *Procedia Manufacturing*, Elsevier B.V., 2017, pp. 778–785. doi: 10.1016/j.promfg.2017.09.184.
- [23] J. L. Prado-Cerqueira, J. L. Diéguez, and A. M. Camacho, “Preliminary development of a Wire and Arc Additive Manufacturing system (WAAM),” in *Procedia Manufacturing*, Elsevier B.V., 2017, pp. 895–902. doi: 10.1016/j.promfg.2017.09.154.
- [24] M. Dinovitzer, X. Chen, J. Laliberte, X. Huang, and H. Frei, “Effect of wire and arc additive manufacturing (WAAM) process parameters on bead geometry and microstructure,” *Addit Manuf*, vol. 26, pp. 138–146, Mar. 2019, doi: 10.1016/j.addma.2018.12.013.
- [25] R. Scharf-Wildenhain, A. Haelsig, J. Hensel, K. Wandtke, D. Schroepfer, and T. Kannengiesser, “Heat control and design-related effects on the properties and welding stresses in WAAM components of high-strength structural steels,” *Welding in the World*, vol. 67, no. 4, pp. 955–965, Apr. 2023, doi: 10.1007/s40194-022-01450-x.
- [26] Z. Hu, X. Qin, Y. Li, and M. Ni, “Welding parameters prediction for arbitrary layer height in robotic wire and arc additive manufacturing,” *Journal of Mechanical Science and Technology*, vol. 34, no. 4, pp. 1683–1695, Apr. 2020, doi: 10.1007/s12206-020-0331-0.
- [27] B. Wu et al., “A review of the wire arc additive manufacturing of metals: properties, defects and quality improvement,” Oct. 01, 2018, Elsevier Ltd. doi: 10.1016/j.jmapro.2018.08.001.

- [28] X. Chen et al., “A review on wire-arc additive manufacturing: typical defects, detection approaches, and multisensor data fusion-based model,” Nov. 01, 2021, Springer Science and Business Media Deutschland GmbH. doi: 10.1007/s00170-021-07807-8.
- [29] J. Ding et al., “Thermo-mechanical analysis of Wire and Arc Additive Layer Manufacturing process on large multi-layer parts,” *Comput Mater Sci*, vol. 50, no. 12, pp. 3315–3322, Dec. 2011, doi: 10.1016/j.commatsci.2011.06.023.
- [30] C. Le Falher, S. Cadiou, S. Morville, M. Courtois, P. Paillard, and P. Le Masson, “Two-Scale Modeling of the WAAM Process: Link Between Thermo-Hydrodynamics and Solid Mechanics.”
- [31] C. Huang, P. Kyvelou, R. Zhang, T. Ben Britton, and L. Gardner, “Mechanical testing and microstructural analysis of wire arc additively manufactured steels,” *Mater Des*, vol. 216, Apr. 2022, doi: 10.1016/j.matdes.2022.110544.
- [32] Ivántabernero, A. Paskual, P. Álvarez, and A. Suárez, “Study on Arc Welding Processes for High Deposition Rate Additive Manufacturing,” in *Procedia CIRP*, Elsevier B.V., 2018, pp. 358–362. doi: 10.1016/j.procir.2017.12.095.
- [33] A. Paolini, S. Kollmannsberger, and E. Rank, “Additive manufacturing in construction: A review on processes, applications, and digital planning methods,” Dec. 01, 2019, Elsevier B.V. doi: 10.1016/j.addma.2019.100894.
- [34] Y. Li *et al.*, “Allocation and scheduling of deposition paths in a layer for multi-robot coordinated wire and arc additive manufacturing of large-scale parts,” *Virtual Phys Prototyp*, vol. 19, no. 1, 2024, doi: 10.1080/17452759.2023.2300680.
- [35] S. Maffia, F. Chiappini, G. Maggiani, V. Furlan, M. Guerrini, and B. Previtali, “Comparison between Eight-Axis Articulated Robot and Five-Axis CNC Gantry Laser Metal Deposition Machines for Fabricating Large Components,” *Applied Sciences (Switzerland)*, vol. 13, no. 9, May 2023, doi: 10.3390/app13095259.
- [36] J. Lan, “Design and Fabrication of a Modular Multi-Material 3D Printer,” 2013.
- [37] A. V. Shembekar, Y. J. Yoon, A. Kanyuck, and S. K. Gupta, “Trajectory Planning for Conformal 3D Printing Using Non-Planar Layers,” *ASME International*, Aug. 2018. doi: 10.1115/detc2018-85975.

- [38] I. Ishak and P. Larochelle, “Robot Arm Platform for Additive Manufacturing: 3D Lattice Structures.”
- [39] A. V. Shembekar, Y. J. Yoon, A. Kanyuck, and S. K. Gupta, “Generating robot trajectories for conformal three-dimensional printing using nonplanar layers,” *J Comput Inf Sci Eng*, vol. 19, no. 3, Sep. 2019, doi: 10.1115/1.4043013.
- [40] F. Wulle, D. Coupek, F. Schäffner, A. Verl, F. Oberhofer, and T. Maier, “Workpiece and Machine Design in Additive Manufacturing for Multi-Axis Fused Deposition Modeling,” in *Procedia CIRP*, Elsevier B.V., 2017, pp. 229–234. doi: 10.1016/j.procir.2017.01.046.
- [41] ICRA2017: IEEE International Conference on Robotics and Automation : program : May 29-June 3, 2017, Singapore. IEEE, 2017.
- [42] G. Zhao, G. Ma, J. Feng, and W. Xiao, “Nonplanar slicing and path generation methods for robotic additive manufacturing,” *International Journal of Advanced Manufacturing Technology*, vol. 96, no. 9–12, pp. 3149–3159, Jun. 2018, doi: 10.1007/s00170-018-1772-9.
- [43] M. Bozorg and A. Khajepour, “ROBUST CONTROLLER DESIGN FOR A GANTRY ROBOT,” 2004. [Online]. Available: <https://www.researchgate.net/publication/273399967>
- [44] M. Habibi and M. Ziadia, “From gantry-based machine to robot-based fused deposition modelling: A state-of-the-art,” 2021, doi: 10.20944/preprints202104.0203.v1.
- [45] N. A. Rosli *et al.*, “Design and development of a low-cost 3d metal printer,” *Journal of Mechanical Engineering Research and Developments*, vol. 41, no. 3, pp. 47–54, 2018, doi: 10.26480/jmerd.03.2018.47.54.
- [46] D. Cuiuri, “Control of the short-circuit gas metal arc welding process using instantaneous current regulation Recommended Citation.” [Online]. Available: <http://ro.uow.edu.au/theses/1944>
- [48] A. Pinar, B. Wijnen, G. C. Anzalone, T. C. Havens, P. G. Sanders, and J. M. Pearce, “Low-cost open-source voltage and current monitor for gas metal arc weld 3D printing,” *J Sens*, vol. 2015, 2015, doi: 10.1155/2015/876714.

- [49] S. Penttilä, H. Lund, and T. Skriko, “Possibilities of Artificial Intelligence-Enabled Feedback Control System in Robotized Gas Metal Arc Welding,” *Journal of Manufacturing and Materials Processing*, vol. 7, no. 3, Jun. 2023, doi: 10.3390/jmmp7030102.

8 APPENDIX

8.1 G-code Samples

2 Layer straight line Code

```

;FLAVOR:Marlin
;TIME:515
;Filament used: 0.646629m
;Layer height: 2
;MINX:149
;MINY:101.5
;MINZ:0.3
;MAXX:151
;MAXY:198.5
;MAXZ:8.3
;Generated with Creality Slicer 4.8.2-291
M104 S200
M105
M109 S200
M82 ;absolute extrusion mode
G28 ;Home
G1 Z15.0 F6000 ;Move the platform down 15mm
;Prime the extruder
G92 E0
G1 F200 E3
G92 E0

G1 F3600 E-6.5
;LAYER_COUNT:5
;LAYER:0
M107
;MESH:Test 3.STL
G0 F900 X151 Y198.5 Z0.3
;TYPE:WALL-OUTER
G1 F3600 E0
G1 F120 X149 Y198.5 E0.28216
G1 X149 Y101.5 E13.96684
G1 X151 Y101.5 E14.249
G1 X151 Y198.5 E23.37212
G0 F900 X150.7 Y198.5
G1 F3600 E16.87212
;MESH:NONMESH
G0 F600 X150.7 Y198.5 Z2.3
G0 F900 X151 Y198.5
;TIME_ELAPSED:117.258108
;LAYER:1
M106 S255
;TYPE:WALL-OUTER
;MESH:Test 3.STL
G1 F3600 E23.37212
G1 F120 X149 Y198.5 E25.25317
G1 X149 Y101.5 E116.48437
G1 X151 Y101.5 E118.36543
G1 X151 Y198.5 E179.18623
G0 F1350 X150.7 Y198.5
G1 F3600 E172.68623
;MESH:NONMESH
G0 F600 X150.7 Y198.5 Z4.3
G0 F1350 X151 Y198.5
;TIME_ELAPSED:216.826611
;LAYER:2
;TYPE:WALL-OUTER
;MESH:Test 3.STL
G1 F3600 E179.18623
G1 F120 X149 Y198.5 E181.06728
G1 X149 Y101.5 E272.29848
G1 X151 Y101.5 E274.17954

```

8.2 Arduino/Marlin/MATLAB Configuration Files/Codes

```
%welding power in watts
P = 3840;

% Power source characteristic parameters
V0 = 100;      % Open circuit voltage
m = -0.125;    % Slope of power source characteristic

%V/I = -m => V = -m * I
%P = V * I => P = (-m * I) * I = -m * I^2

% Solve for I
I_opt = sqrt(P / (-m));      % Optimal current
V_opt = -m * I_opt;          % Optimal voltage

% Display results
fprintf('Power: %.2f W\n', P);
fprintf('Optimal Current: %.2f A\n', I_opt);
fprintf('Optimal Voltage: %.2f V\n', V_opt);
```

Figure 8.1: MATLAB code

```
clc; clear; close all;

I = linspace(80, 260, 10); %Define welding current range

V_sheath = 12;      % Vc + Va
R_ext = 0.005;      % Resistance of extension
E_arc = 1.5;        % Arc voltage per unit length [V/mm]

feed_rates = [1,1.5,2,2.5,3,3.5,4,4.5,5,5.5,6]; % Wire feed rates [m/min]
base_voltage = 21.91; % Base arc voltage
voltage_slope = 0.5; % Arc voltage increase per m/min of WFR

colors = lines(length(feed_rates));

figure;
hold on;

for k = 1:length(feed_rates)
    WFR = feed_rates(k);

    % Estimate arc voltage for this feed rate
    U = base_voltage + voltage_slope * (WFR - min(feed_rates));

    % Compute arc length for each current
    L = (U - V_sheath - I .* R_ext) ./ E_arc; % Arc Length in mm

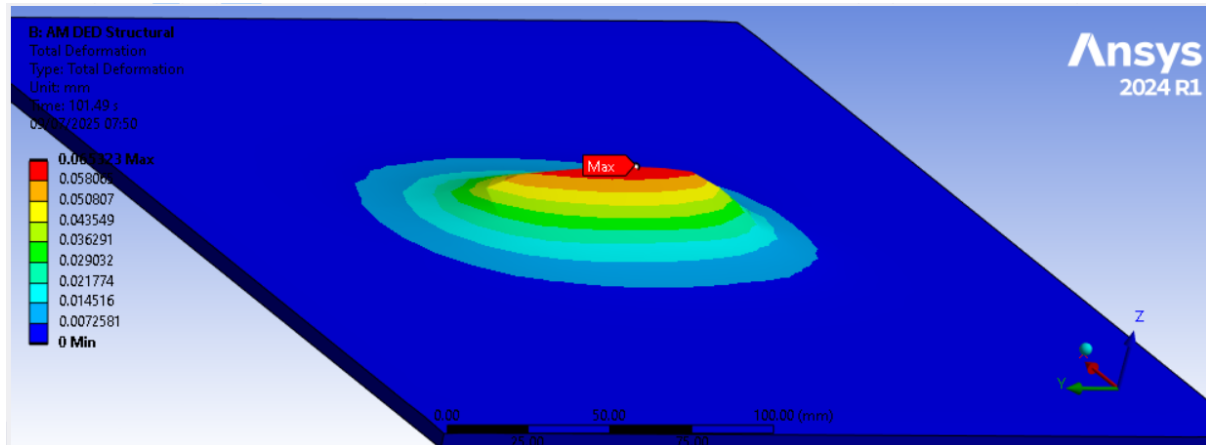
    plot(I, L, 'LineWidth', 2, 'Color', colors(k,:), ...
         'DisplayName', sprintf('WFR = %d m/min', WFR));
end

xlabel('Welding Current (A)', 'FontSize', 12);
ylabel('Arc Length (mm)', 'FontSize', 12);
title('Arc Length vs Welding Current at Different Wire Feed Rates (MIG)', 'FontSize', 14);
legend('Location', 'northeast');
grid on;
xlim([80 260]);
```

Figure 8.2: MATLAB code to find the suitable arc lengths in different arc currents

8.3 Simulation Screenshots and Mesh Data

Simulation for 2-layer rectangular weld bead



Total Deformation

Simulation for 5-layer rectangular weld bead

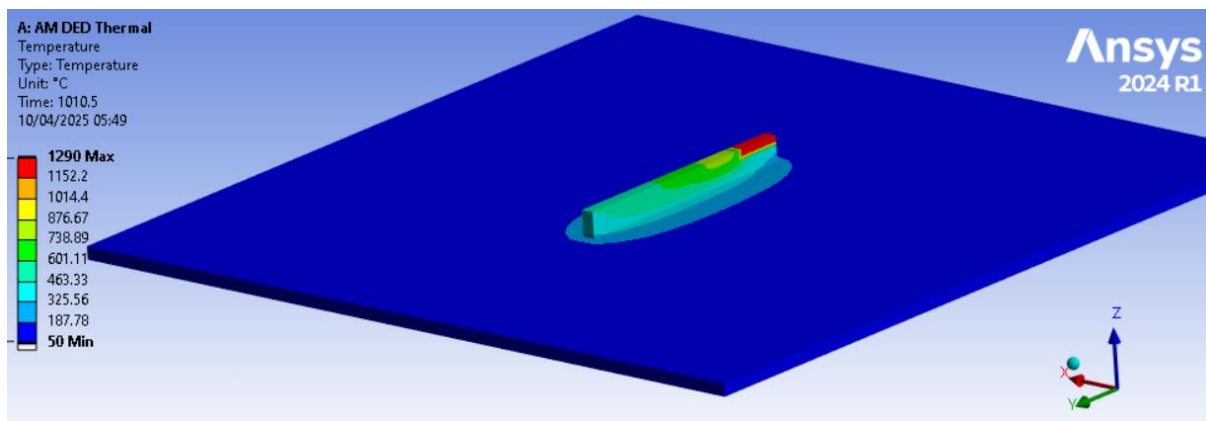


Figure 8.3: Thermal Simulation

8.4 CAD Drawings and Wiring Diagrams

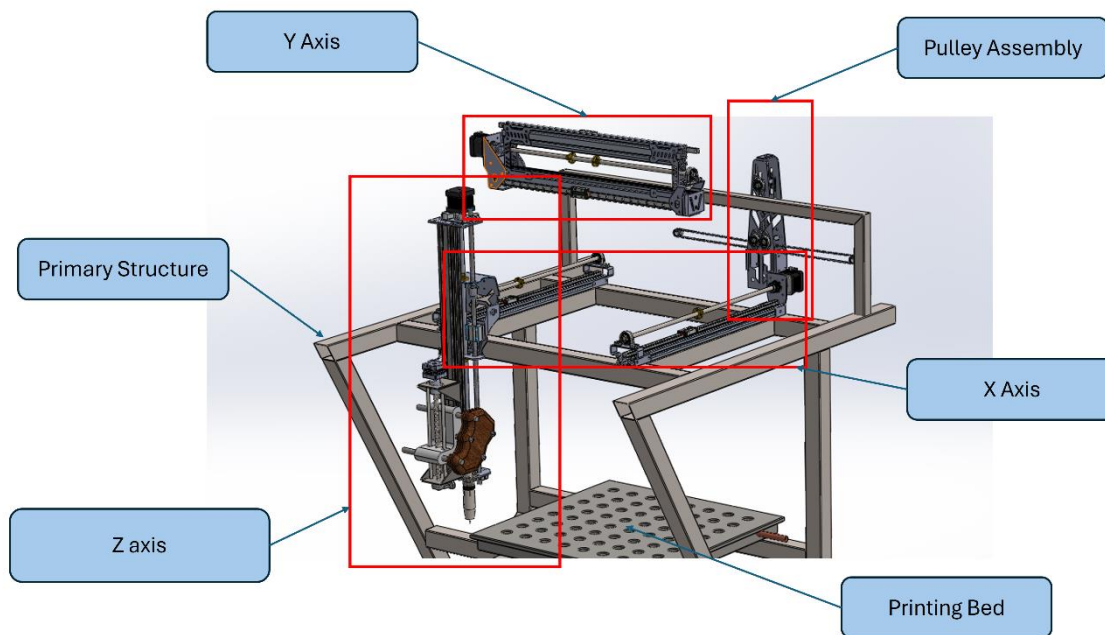


Figure 8.4: CAD Model

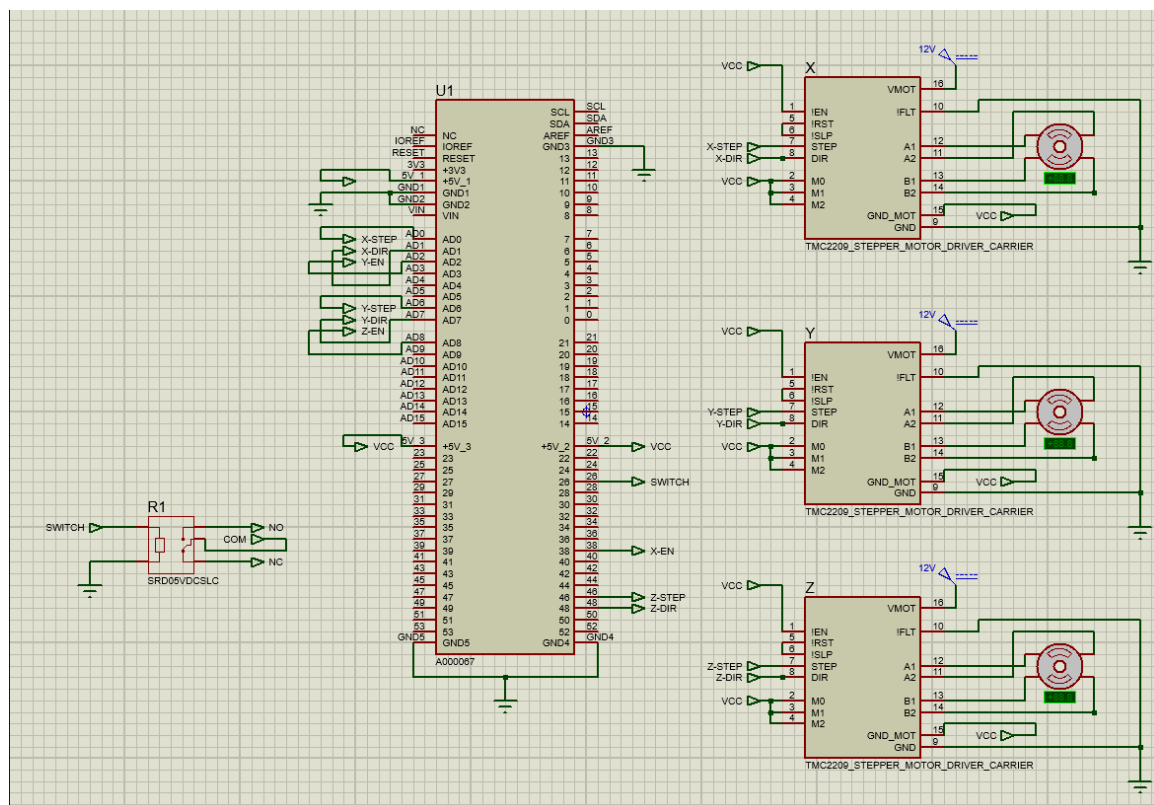


Figure 8.5: Gantry Control System

8.5 Images of the Manufactured Prototype



Figure 8.7: Steel Box Bar Structure



Figure 8.6: Fully Assembled Prototype



Figure 8.8: Front View of Assembly

8.6 Raw Experimental Data

Manual Welds

Type	Code
Torch Angled - Box	T001
Torch Perpendicular to Plate - Box	T002
Travel Speed 1 - Straight Line	T003
Travel Speed 2 - Straight Line	T004
Current value 1 - straight line	T005
Current value 2 - straight line	T006
Current value 3 - straight line	T007
Voltage value 1 - Straight line	T008
Voltage value 2 - Straight line	T009
Voltage value 3 - Straight line	T010
Arc Length Value 1	T011
Arc Length Value 2	T012
Arc Length Value 3	T013
Arc Length Varying	T014



Figure 8.10 : T001 Welding position 30-degree angle



Figure 8.9 : T002 Welding position 90-degree angle

le



Figure 8.16: T001 Rectangular box in torch 30-degree angled



Figure 8.11 : T002 Rectangular box in torch 90-degree perpendicular



Figure 8.13: T005, T006 and T007 Welding bead



Figure 8.12: T008, T009 and T0019 Welding beads



Figure 8.19: T011, T012, T013, T014 Welding Beads

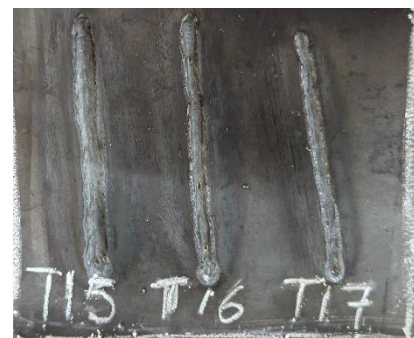




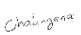
Figure 8.20: T015, T016, T017 Welding Beads

Report Submission
Changes to the First Submission
ME4204

Group No 31

**DESIGN AND DEVELOPMENT OF A METAL
ADDITIVE MANUFACTURING SYSTEM TO
FABRICATE COMPONENTS**

By

Index No.	Name	Signature
200159X	S.C.P. Ephraims	
200024F	K.S. Amarasekara	
200055B	A.G.C.O. Atadaswala	

Advisors' names, associations and signature

Prof. Nirosh Jayaweera	Department of Mechanical Engineering, University of Moratuwa	
Dr. Eranga De Silva	Department of Mechanical Engineering, University of Moratuwa	

Department of Mechanical Engineering
University of Moratuwa
Sri Lanka

#	Pages	Changes carried out
1	54	Welding torch activation section was changed into a new method
2	41	Torch mount image was changed
3	59-65	Results and Discussion section and Conclusion section was completely changed with updated results.
4	All pages	Image caption font sizes were increased
5	37	Heading 4.1 was added.
6	All pages	Table captions were corrected